Combustion and Flame 197 (2018) 49–64

Contents lists available at ScienceDirect

Combustion and Flame

journal homepage: www.elsevier.com/locate/combustflame

Experimental and chemical kinetic modeling investigation of methyl butanoate as a component of biodiesel surrogate

Aditya D. Lele[a], Sonal K. Vallabhuni[b], Kai Moshammer[b], Ravi X. Fernandes[b], Anand Krishnasamy[a], Krithika Narayanaswamy[a,*]

[a] Department of Mechanical Engineering, Indian Institute of Technology Madras, Chennai 600036, India
[b] Physikalisch-Technische Bundesanstalt, Bundesallee 100, Braunschweig 38116, Germany

ARTICLE INFO

Article history:
Received 26 January 2018
Revised 27 June 2018
Accepted 27 June 2018

Keywords:
Methyl esters
Methyl butanoate kinetics
Skeletal model
Rapid compression machine
Biodiesel surrogate

ABSTRACT

Biodiesel is a potential alternative to fossil diesel. In combustion simulations, in order to circumvent the difficulty in integrating reaction schemes for biodiesels, which are typically of a large size and not well understood, a surrogate approach to simplify the representation of its long chain methyl ester components is adopted. In this work, a compact reaction scheme for methyl butanoate, which is a potentially important candidate for biodiesel surrogates, is derived from a detailed reference mechanism (Dooley et al., 2008). An existing well-validated model for *n*-dodecane (Narayanaswamy et al., 2014) oxidation, which is a suitable base to model biodiesel surrogates, is augmented with the oxidation pathways of methyl butanoate. The resulting combined mechanism is comprehensively assessed for methyl butanoate kinetic description. Several rate constants pertaining to methyl butanoate kinetics are updated in the resulting chemical mechanism based on recent rate recommendations from the literature in a consistent manner. The revised kinetic model has been validated comprehensively against a wide range of experimental data and found to be satisfactory. In addition, auto-ignition delay times of methyl butanoate have been measured in a rapid compression machine (RCM). The ignition delay time measurements cover a wide range of experimental conditions: temperatures of 850–1100 K and pressures of 10–40 bar. The impact of varying equivalence ratios on ignition delay times has also been investigated for ϕ = 0.5–1.5 and ignition delay times are reported for the rich mixtures for the first time as a part of this work. No two-stage ignition or negative temperature coefficient (NTC) behavior has been observed for methyl butanoate in the experimental investigation. The effect of addition of low-temperature chemistry pathways to the methyl butanoate chemical kinetic mechanism has also been explored.

1. Introduction

Increase in the use of renewable alternative fuels will decrease our dependence on fossil fuels and help reduce greenhouse gas emissions. Biodiesel is one such potential alternative to partially or completely replace fossil diesel [1]. It consists of long chain saturated as well as unsaturated methyl esters ranging from C_{14}–C_{24} [2]. These constituents are present in varied compositions based on the source of biodiesel. A detailed kinetic mechanism developed for these constituents runs into several thousands of species and reactions [3]. To circumvent the difficulty in utilizing such a large kinetic scheme in engine simulations, several studies have investigated the use of various surrogates for biodiesel [4–9], which have been recently summarized in Ref. [10].

In developing a reaction mechanism for a surrogate fuel, it is crucial to capture the component kinetics accurately in order to make meaningful assessment about suitability of the surrogate to represent the real fuel. Thus, although methyl decanoate has been used in recent studies [7–9] as a surrogate component owing to its ability to reproduce the reactivity, negative temperature coefficient (NTC) behavior, and early CO_2 rise, characteristic to the long chain methyl esters in biodiesels, methyl butanoate (MB), which is the most comprehensively investigated methyl ester in terms of kinetic studies [11], is selected here to represent the ester content in biodiesels. Methyl butanoate has not been found to exhibit any NTC behavior in the conditions where longer esters did show NTC behavior and it lacks the reactivity characteristic of long chain ester molecules. Nonetheless, methyl butanoate, in combination with *n*-alkanes is found to predict combustion and

* Corresponding author.
E-mail addresses: krithika@iitm.ac.in, krithika.n@alumni.stanford.edu (K. Narayanaswamy).

https://doi.org/10.1016/j.combustflame.2018.06.033
0010-2180/

emission characteristics of biodiesel [19], which can therefore be considered as a promising candidates for biodiesel surrogates.

Fisher et al. [12] developed the earliest model for methyl butanoate oxidation and validated it against pressure measurements in a constant volume chamber. Their model exhibited a weak NTC and was in qualitative agreement with the available experimental data at that time. Several detailed mechanisms have been developed [11,13–15] thereafter, along with a wide variety of experimental studies for auto-ignition and pyrolysis of methyl butanoate [11,15,29,56–58] and its flames [13,37,46,47]. These kinetic descriptions are mainly derived from the relatively well understood alkane kinetics by accounting for ester specific effects.

Dooley et al. [11] developed a comprehensive reaction mechanism for methyl butanoate and validated it against a wide range of experiments. This model did not include any low-temperature chemistry pathways. Gail et al. [13,16] performed an experimental and kinetic modeling study of methyl butanoate and methyl crotonate. They investigated the effects of unsaturation and identified reaction pathways responsible for differences between saturated and unsaturated methyl ester. Hakka et al. [15] generated a detailed kinetic mechanism for methyl butanoate using the mechanism generation software EXGAS [17]. Gail et al. [13] and Hakka et al. [15] models included the pathways for low-temperature oxidation of methyl butanoate although NTC behavior has not been observed in any of the existing auto-ignition experiments.

Complementing the kinetic modeling efforts, several researchers have examined methyl butanoate kinetics using theoretical techniques [18–24]. Huynh et al. [25] developed a sub-mechanism for methyl butanoate based on a detailed ab-initio study. This sub-mechanism was verified against shock tube pyrolysis experiments. Some researchers [20,21,26] also investigated the important reactions for auto-ignition such as H-atom abstraction from methyl butanoate by different radicals using different levels of theories. Low-temperature chemistry pathways important for methyl butanoate oxidation have also been explored recently [22,23] using quantum chemical calculations. Although no NTC behavior is observed, these studies suggest that the inclusion of low-temperature oxidation pathways might be important for predicting auto-ignition at low temperatures.

Auto-ignition of methyl butanoate has already been investigated experimentally using shock tubes and rapid compression machines (RCM). Dooley et al. [11] measured ignition delays of methyl butanoate in a shock tube (P = 1,4 bar, T = 1250–1760 K and ϕ = 0.25–1.5) and RCM (P = 10–40 bar, T = 640–949 K and ϕ = 0.33–1.00). Hakka et al. [15] also studied auto-ignition of methyl butanoate in shock tube at higher pressure (P = 8 bar, T= 1250–2000 K and ϕ = 0.25–2). Additional measurements of ignition delays have also been obtained in RCM facilities [27–29]. Of these, Kumar and Sung [29] have recently explored a wide range of conditions (P = 15–75 bar, T = 833–1112 K and ϕ = 0.25–1.00). Notably, auto-ignition of rich MB mixtures has not been investigated yet at intermediate temperature (850 K $<$ T $<$ 1100 K) under engine relevant conditions.

The primary goal of this work is to: (a) present additional auto-ignition data for methyl butanoate at conditions not investigated earlier along with (b) a compact reaction scheme for methyl butanoate oxidation, yet thoroughly examined for its kinetic description and validated against an array of experimental configurations. This work is organized as follows. Firstly, ignition delay time measurements for MB in a rapid compression machine covering a wide range of operating conditions (P = 10–40 bar, T = 850–1100 K and ϕ = 0.5–1.5) are presented in Section 2. It is to be highlighted that ignition delays for rich MB mixtures are reported for the first time in the intermediate temperature (850–1100 K) regime, thereby providing valuable data for kinetic model validation at these conditions. Thereafter, the development of the kinetic scheme is described in Section 3. The oxidation pathways of methyl butanoate are derived from a detailed mechanism [11] and incorporated into a well-characterized model for n-dodecane oxidation [30], considering the potential of this long chain alkane as a component of a possible biodiesel surrogate [19,63,64]. The kinetic description of methyl butanoate oxidation in the resulting mechanism is revised and updated based on rate parameter recommendations for methyl butanoate oxidation from recent theoretical studies, which have not been utilized yet for model development. The proposed model is then comprehensively validated against available methyl butanoate experimental data as well as the new data-sets obtained in the present work (Section 4). The revised model is found to Result in improved model predictions for methyl butanoate.

The existing set of experiments, including the ones presented in this work, do not show NTC or two-stage ignition. Nonetheless, the addition of low-temperature chemistry pathways has also been explored here for completeness. Since the validity of the low-temperature model cannot be ascertained with the available experimental data, this discussion is presented separately in Section 5. This investigation points toward potential experimental studies required to assess the low-temperature chemistry of methyl butanoate in future.

2. Experimental methodology

The rapid compression machine used in this study is located at Physikalisch-Technische Bundesanstalt (PTB), which is similar to that used by Mittal and Sung [31]. It consists of a single piston design, where a pneumatically driven and hydraulically controlled creviced piston compresses the mixture inside the reaction chamber to a desired end of compression pressure (P_C) and temperature (T_C). The reaction chamber has a maximum working pressure of 200 bar and an operating temperature range of 600–1100 K. The rapid compression machine has been designed to obtain a wide range of compression ratios with adjustable stroke length and clearance. A compression ratio of 25.6:1 has been used in this study.

The test mixtures were prepared manometrically in a stainless-steel tank at the room temperature by using a 5000-mbar barometer (MKS Baratoron) to an accuracy of $\pm$1 mbar to measure the partial pressures of the gases. The steel tank is cleaned with the bath gases to remove impurities prior to filling of the constituent gases. Methyl butanoate (99%, Sigma Aldrich) is used as a fuel for autoignition. Different combinations of argon (99.999%) and nitrogen (99.999%) are used as bath gases in RCM experiments to obtain the appropriate value of ϕ and different end of compression temperatures T_C. A small mass of methyl butanoate is introduced into the evacuated mixing tank via a septum by means of a syringe, such that its partial pressure is well below its vapour pressure. Oxidizer (99.999% purity O_2) and diluent gases are added manometrically according to the mixture composition. These gaseous mixtures are allowed to mix in the steel tank for at least 12 hours before transferring to the reaction chamber to ensure homogeneity. Table 1 lists the mixture compositions used in the experiments. Along with the use of different diluent gases, preheating is also used to obtain desired T_C. Uniform heating of reaction chamber, mixing cylinder and gas filling assembly has been ensured for this purpose by using a combination of heating tapes and temperature monitoring using Pt-Rh thermocouples. This entire arrangement was insulated to avert the formation of any cold spots.

Owing to the difficulty of directly measuring the temperature inside the reaction chamber, T_C is determined assuming an adiabatic core using GasEq [32] as,

$$\int_{T_0}^{T_C} \frac{\gamma}{\gamma - 1} \frac{dT}{T} = \ln\left(\frac{P_C}{P_0}\right), \tag{1}$$

Table 1
Mixture compositions, temperature and pressure ranges for RCM experiments.

Mix	Fuel	O_2	Ar	N_2	ϕ	Temperature range (K)	Pressure (bar)
(Mole fractions)							
1	0.01	0.1300	0.7309	0.1289	0.50	1016–1083	10, 15, 20
2	0.01	0.1300	0.5589	0.3009	0.50	966–1005	15, 20
3	0.01	0.1300	0.4299	0.4299	0.50	886–954	30, 40
4	0.02	0.1300	0.6969	0.1529	1.00	922–959	20
5	0.02	0.1300	0.5949	0.2549	1.00	884–982	15, 20, 30
6	0.01	0.0433	0.3786	0.5679	1.50	890–948	40
7	0.01	0.0433	0.5206	0.4259	1.50	919–1073	20, 30

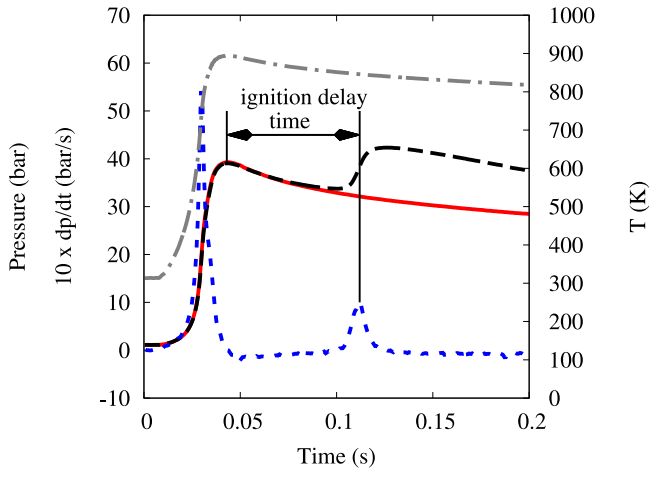

Fig. 1. Characteristic pressure signal for an RCM experiment. Solid line : Pressure signal for non-reactive mixture; Dashed line : Pressure signal for reactive mixture; Dotted line : First derivative of reactive pressure signal (scaled up); Dash-dotted line: Computed temperature corresponding to non-reactive pressure. Details of the experiment are as follows: P_0= 1100 mbar, T_0 = 313 K, P_c= 40 bar, T_c = 890 K, ϕ = 1.50 and Mix-6 composition (see Table 1).

where T_0 and P_0 represent initial temperature and pressure respectively, and γ is the ratio of specific heats for the initial mixture which is a function of temperature. Reaction chamber pressure is measured using a Kistler (601H) pressure transducer flush with the inside wall of the reaction chamber. The pressure signal is recorded with the use of a charge amplifier (Type 5018) and a spectrum data acquisition card (M2i.3016-Exp). The time resolved pressure signal is further processed to determine the ignition delay time.

Figure 1 shows a typical pressure signal recorded for an ignition event along with the pressure trace for the corresponding non-reactive mixture. The pressure signals have been post-processed using an in-house MATLAB code to eliminate the noise and account for the offset of pressure transducer similar to Ref. [33]. This processed signal is then used to determine the ignition delay time, which has been defined as the time between the end of compression and the maximum rate of pressure rise during the ignition event as shown in Fig. 1. For each ignition delay time measurement at every operating condition, a corresponding non-reactive pressure signal was measured by using a non-reactive mixture obtained by replacing O_2 in the reactive mixture with N_2. This non-reactive pressure signal is used to account for the compression as well as post compression heat losses while simulating these experiments. As a result, the computed temperature shows a gradual decrease in the post-compression zone.

Ignition delay time measurements have been found to be repeatable within 20% for all the conditions examined here. Every measurement has been repeated at least twice with most of them repeated three times. The ignition delay time data represents the average value estimated over the multiple repetitions for the same experimental condition. The uncertainty for the temperature at the end of the compression was calculated by considering an independent parameter methodology by linearizing the equation for T_c and applying the method of quadratic sums [60]. A detailed explanation can be found in Weber et al. [61].

$$\delta T_c = 2\sqrt{\sum_{k=T_0,P_0,P_c}\left(\frac{\delta T_c}{\delta k}\sigma_k\right)^2}$$

where δT_c is the total uncertainty in T_c, σ_k is the standard deviations of parameter k. The coverage factor of δT_c is 2 such that the confidence interval is 95.4%, if the distribution of the total uncertainty is assumed to be normal. The standard deviation of the three parameters ($\sigma_{T_0}, \sigma_{P_0}, \sigma_{P_c}$) are estimated from manufacturer's specifications and this translates to δT_c for mixture consisting of nitrogen to be 5 K and 10 K for that consisting of argon. Based on the mixture composition, the value thus varies between 5–10 K.

3. Kinetic model development

3.1. Skeletal mechanism

Starting with a detailed reaction scheme for methyl butanoate oxidation (275 species, 1545 reactions) proposed by Dooley et al. [11], a compact mechanism is derived using the DRGEP [34] method. The database used to carry out mechanism reduction includes homogeneous isochoric reactor configurations at low to high temperatures $T = 700$–1500 K, pressure $P = 13.5$ bar, and equivalence ratio ϕ=1. The resulting reduced mechanism consists of 89 species and 560 reactions. Figure 2 shows a comparison between the detailed [11] and the skeletal kinetic model for a representative case. Similar agreement has been found for conditions spanning a temperature range of 700–1500 K, a pressure range of 1–40 bar, and equivalence ratios of 0.5–1.5 with the maximum error between the skeletal model and the reference mechanisms being $< 5\%$. Additional comparisons can be found in the supplementary material (see Fig. S1).

Considering the potential of a long chain *n*-alkane as a component of a possible biodiesel surrogate [19,63,64], the MB skeletal mechanism is first augmented to a well-characterized kinetic model for *n*-dodecane oxidation. This approach is similar to the methodology adopted in our earlier work [62] to develop a kinetic model for jet fuel surrogates. The kinetics of *n*-dodecane (DD) are taken from the reaction mechanism proposed by Narayanaswamy et al. [30]. The mechanisms for MB and DD are combined using an interactive tool [35] that automatically identifies common species and reactions from the different mechanisms, and incompatibilities between the kinetic data sets. In the combined mechanism, the base chemistry ($C_1, C_2, H_2 - O_2$) is retained from the *n*-dodecane mechanism [30] and duplicate pathways and species have been removed to ensure consistency between the component sub-mechanisms.

The combined mechanism is compared with the reference methyl butanoate mechanism [11] and shown here (see Fig. 3) for

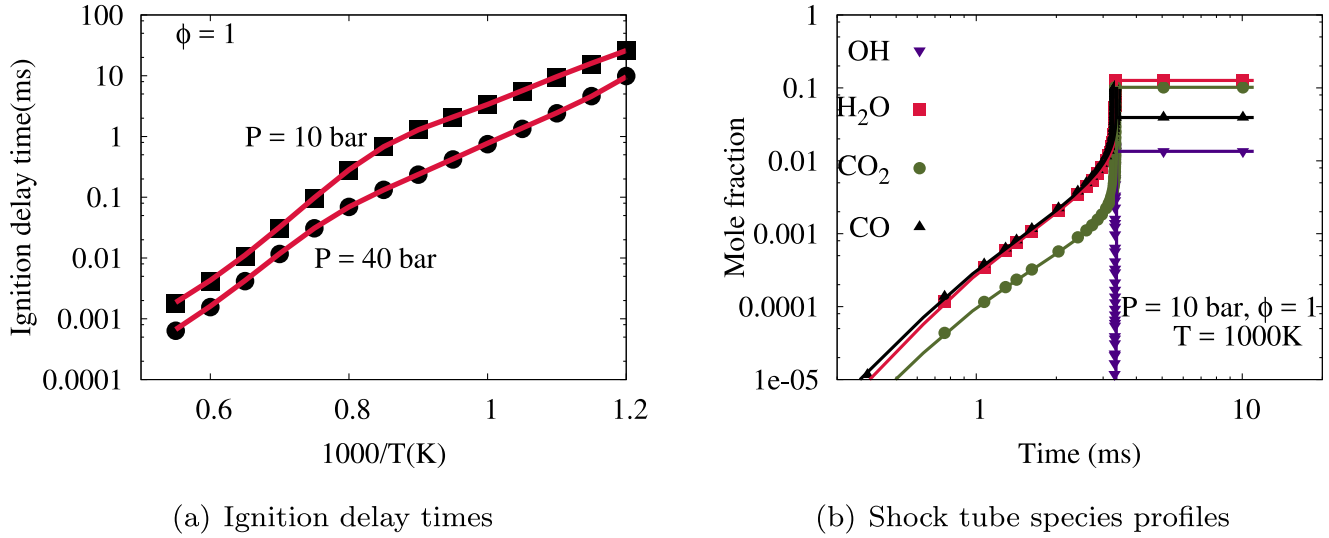

(a) Ignition delay times (b) Shock tube species profiles

Fig. 2. Comparison of the computed results obtained using (i) the detailed mechanism[11] (Symbols) comprising 275 species and 1545 reactions and with (ii) the skeletal mechanism (Solid lines) derived using DRGEP [34] consisting of 89 species and 560 reactions for: (a) ignition delay times of MB/air mixtures and (b) species profiles in a isochor homogeneous reactor for MB/air oxidation.

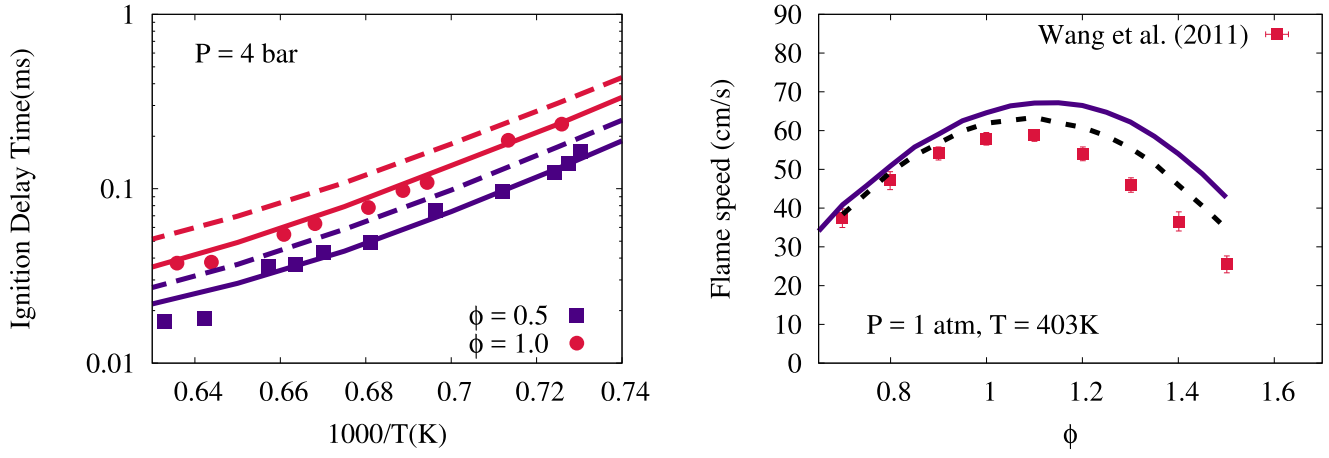

(a) Ignition delay times (b) Laminar burning velocities

Fig. 3. Results for (a) ignition delay times of methyl butanoate and (b) laminar burning velocities of methyl butanoate; symbols : Experiments [11,37]; lines : (i) parent methyl butanoate [11] mechanism (Solid lines) and (ii) combined methyl butanoate + *n*-dodecane (DD) mechanism (Dashed lines). The uncertainties in the reported experiments are same as the size of the symbols used to represent the data.

two representative experimental data sets, namely, (i) ignition delays in shock tubes and (ii) laminar burning velocities. The combined mechanism shows lesser reactivity compared to the reference MB mechanism [11] in Fig. 3(a).

To investigate the differences in ignition delays between the detailed MB mechanism and the combined mechanism, ignition delays were recomputed using a combined mechanism derived by retaining the base chemistry from the reference MB mechanism. The simulated ignition times are found to agree with the parent mechanism (not shown here) suggesting that the differences shown in Fig. 3(a) can be attributed to collective effect due to choice of the base chemistry. Nevertheless, a comparison of flame speeds depicted in Fig. 3(b) shows that the combined mechanism displays better agreement with the experimental data compared to the reference mechanism. It is well known that laminar flame speed predictions are very much sensitive to reactions among small species pertaining to C_0–C_3 kinetics. Thus, this observation suggests that the base chemistry, which has been comprehensively validated [30,36] previously, is already appropriate, and points to the need to refine the methyl butanoate sub-mechanism to improve upon its kinetic description.

The following subsection discusses the revisions to the MB sub-mechanism followed by a discussion on the predictive capabilities of the updated model.

3.2. Modifications to the reaction mechanism

In the reference MB mechanism [11], rate constants are primarily derived using the reaction class approach [38,39], employing well studied *n*-alkane kinetics for rate constant estimation. Rate parameters have been assigned based on the similarity between types of C atom present in MB and *n*-alkanes, which has already been discussed in Ref. [11]. Though this approach has been instrumental in the development of reaction mechanisms for different classes of hydrocarbons, theoretical studies on the actual molecule certainly provide more accurate values of rate parameters specific to the pathways involving the species of interest. Therefore, theoretical investigations on MB kinetics that have become available

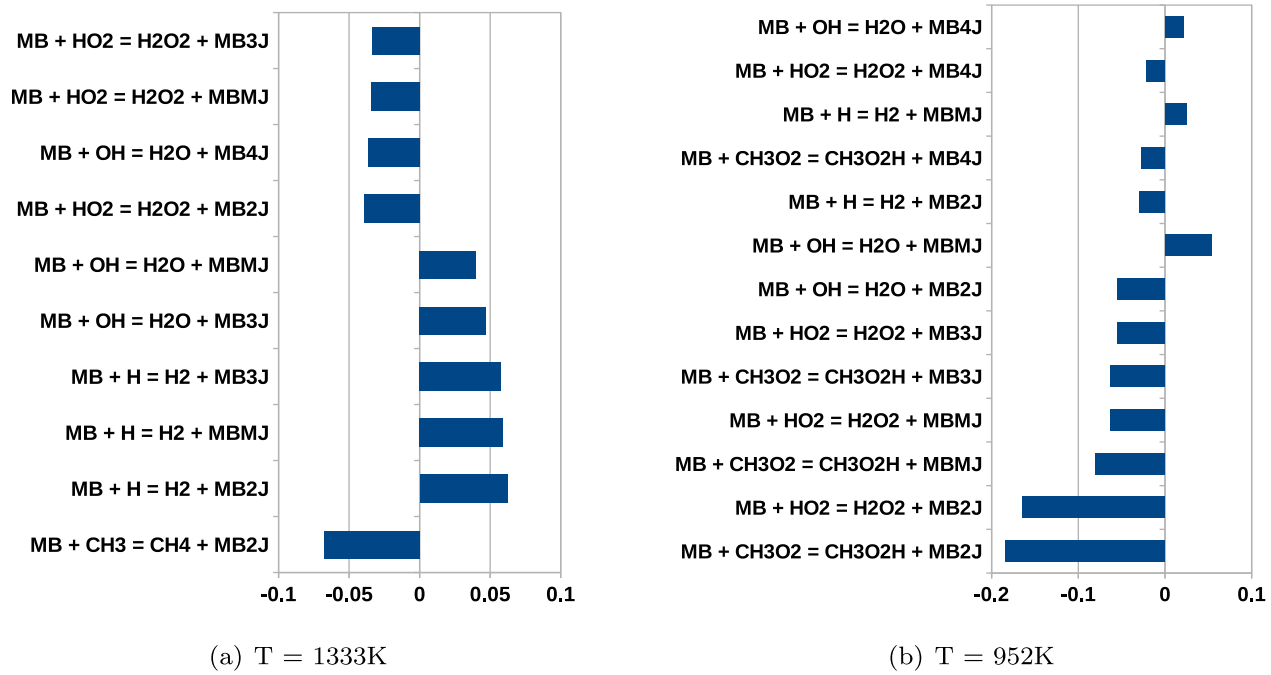

Fig. 4. Sensitivity analysis for ignition delays of MB/air mixture at P= 10 bar and $\phi = 1$ using the detailed MB mechanism [11]. Sensitivities are determined by multiplying each rate constant by a factor of 2, and finding the corresponding change in ignition delays. Only fuel specific reactions having uncertainties greater than 0.02 are shown here.

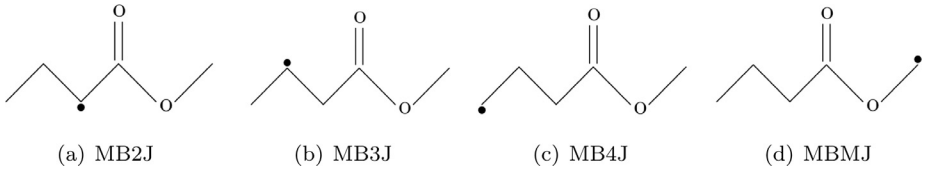

Fig. 5. Radicals resulting from the abstraction of H-atom in methyl butanoate at different sites.

recently [18,20,21,26] have been utilized in the development of the kinetic scheme described below.

3.2.1. MB thermal decomposition submodel

Firstly, the MB decomposition model from Huynh and Violi [18] is incorporated into the combined model. In their ab-initio study [18], RRKM and transition state theories were used to determine rate constants for pathways important to MB decomposition. This submodel consists of thirteen pathways composing of the thermal decomposition of MB into smaller species and their subsequent reactions. Most of these reactions are already a part of the combined mechanism and very few additional reactions are required (see supplementary materials, Table 1) to completely incorporate the Huynh and Violi [18] MB thermal decomposition submodel into the combined model. This lends further confidence in the extent of reduction performed in deriving the skeletal MB submodel and assures that it includes the pathways important for high temperature oxidation of methyl butanoate.

3.2.2. H-atom abstraction by H, OH, CH_3 and HO_2

Figure 4 shows the sensitivity of auto-ignition towards rates of fuel specific reactions using the reference MB mechanism [11] at intermediate (T = 952 K) and high temperatures (T = 1333 K) for an isochor homogeneous reactor. H-atom abstraction by different radicals are by far the most important reactions for these configurations. Hence, their rates play a key role in the predictions of ignition delay times.

H-atom abstraction by H from MB is an important class of reactions for the formation of the initial radical pool at high temperatures (T > 1200 K) affecting auto-ignition and flame speeds. Their rates have been investigated theoretically by several studies [18,19,24,26] employing different levels of theories. In this study, we have incorporated the most accurate rate constants from Zhang et al. [26] calculated using Master equation analysis. A comparison of these rate constants from different sources has been discussed elsewhere [26]. It has been observed that H-atom abstraction from the carbon site adjacent to the carbonyl C has the lowest energy barrier owing to the formation of the resonantly stabilized allyl radical MB2J (see Fig. 18). Hence, the formation of the MB2J radical is energetically favored over other fuel radicals. For example, the formation of MB2J through H abstraction by OH radical is 1.5–1.7 times higher than the formation of MB3J radical through a similar pathway over a temperature range of 700–2000 K. The rates for H-atom abstraction by CH_3 and OH are taken from Refs. [18] and [21] respectively, in the combined mechanism.

At intermediate temperatures (800 K < T < 1000 K), ignition delays are very sensitive to H-atom abstraction by HO_2 (see Fig. 4(b)). Upon abstraction of H-atom from MB by HO_2, H_2O_2 radical is formed, which is a meta-stable species. It leads to chain branching by decomposing into two OH radicals when the system temperature crosses a particular threshold ($T \sim$ 1000 K) [40]. These rate constants have been updated based on the high pressure limit rate constants calculated by Mendes et al. [20]. Abstraction by CH_3O_2 radical has been treated similar to that of HO_2, as suggested by Sarathy et al. [41]. The sensitivity of ignition delay times towards H-atom abstraction in the intermediate temperature range (800–1000 K) by HO_2 and CH_3O_2 is so significant, that changing in these rate constants within their uncertain-

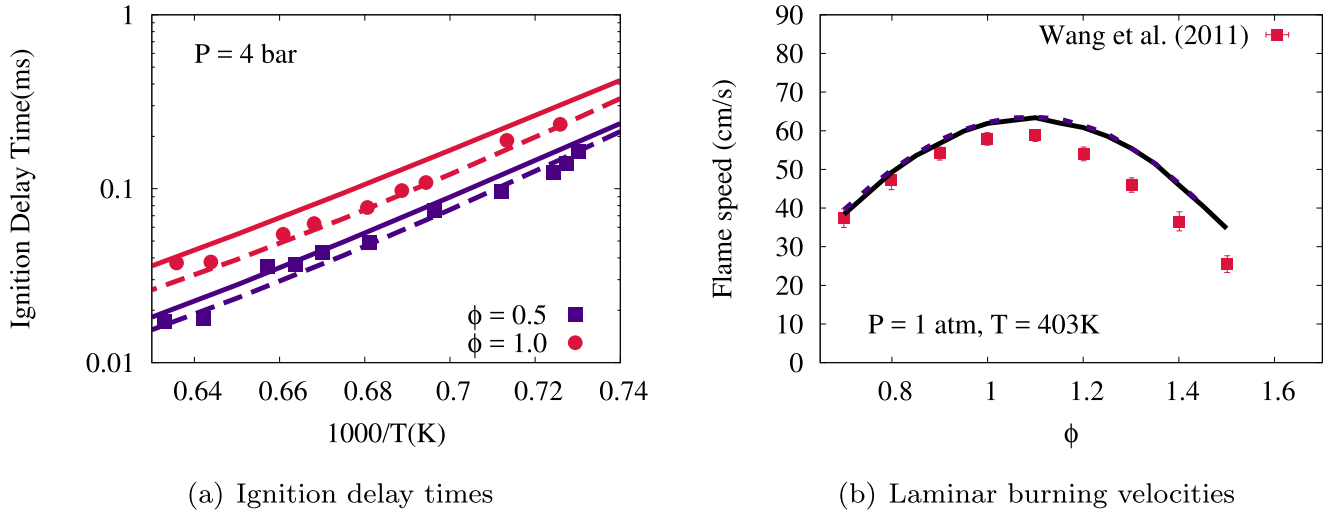

(a) Ignition delay times (b) Laminar burning velocities

Fig. 6. Results for ignition delay times and laminar burning velocities; symbols : experiments [11,37]; lines : (i) methyl butanoate model before revisions (Solid lines) and (ii) methyl butanoate model after revisions (Dashed lines) (same as IITM high T model). The uncertainties in the reported experiments are same as the size of the symbols used to represent the data.

Table 2
List of all the experiments used for the validation of the IITM high T model.

Homogeneous reactors				Flames	
Ignition delay times		Species profiles		Flame speeds	Species profiles
Shock tube	RCM	JSR	VPFR		Laminar flat flame
Dooley et al. [11] Hakka et al. [15]	Kumar and Sung [29] This study	Gail et al. [13]	Marchese et al. [45]	Wang et al. [37] Liu et al. [47]	Yang et al. [46]

ties can affect the ignition delay time predictions by 20–50% (see supplementary materials, Figs. S2 and S3). We found that enhancing the rate constants for H-atom abstraction by HO_2 by a factor of 2, which is within the uncertainty of factor of 2.5 for this class of reactions [20], helps the model to predict ignition delays better at these temperatures.

3.2.3. Effect of rate constant updates

The changes discussed above involve most of the important reactions for thermal decomposition and auto-ignition of MB. The MB submodel is now based on rate parameters drawn from theoretical calculations whenever available. The combined kinetic model consisting of all the above changes is referred to as *IITM high T model* henceforth.

Simulations performed with the combined mechanism are presented in Fig. 6 (with and without the rate constant modifications) for two representative cases of auto-ignition and premixed flames. The updated model predicts ignition delay times in good agreement with the measurements at high temperatures ($T > 1200$ K), displaying an improvement over the results obtained using the combined mechanism. Increase in the reactivity of the updated mechanism at high temperatures (see Fig. 6(a)) can be mainly attributed to the changes in rate constants used for H-atom abstraction by H and OH radicals from the theoretical studies [21,26]. It should be noted that the change in these rate constants make little difference to the laminar flame speeds (see Fig. 6(b)).

Compared to the reference mechanism [11], the model proposed here includes improved base chemistry derived from the DD [30] model along with changes in MB rate parameters as discussed above. Comparison with additional experimental configurations are deliberated in the forthcoming sections.

The IITM high T model consists of 275 species and 2431 reactions (counting forward and backward reactions together). The results for *n*-dodecane in the combined mechanism after revisions

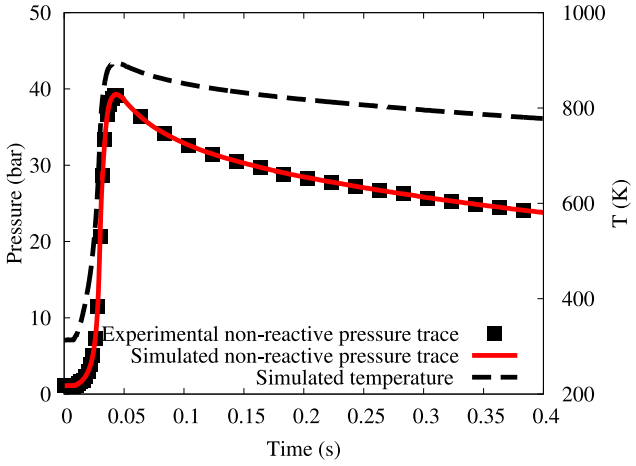

Fig. 7. Comparison between the experimental pressure signal (square symbols) after accounting for the pressure offset and the simulated pressure profile (solid line) as well as temperature (dashed line) generated using volume profile.

to methyl butanoate chemistry have also been verified to be similar to those in Narayanaswamy et al. [30] (see supplementary materials, Fig. S10). The thermodynamic and transport properties for the base chemistry as well *n*-dodecane specific species has been derived from a reference *n*-dodecane [30] mechanism. However, the thermodynamic and transport properties for species related to methyl butanoate kinetics are taken from a reference methyl butanoate [11] mechanism. The proposed reaction mechanism, along with the corresponding thermodynamic and transport properties have been included in the supporting materials.

Table 3
List of configurations used to simulate different experiments.

Experiments	Simulations
Shock tube	Isochoric and adiabatic homogeneous reactor (FlameMaster [42])
Rapid compression machine	Homogeneous reactor with prescribed volume profile (CHEMKIN [43])
Jet stirred reactor	Perfectly stirred reactor at isothermal conditions (FlameMaster [42])
Twin flame premixed	Unstretched and adiabatic premixed flame (FlameMaster [42])
Variable pressure flow reactor	Isobaric and adiabatic homogeneous reactor (FlameMaster [42])
Flat flame burner	Unstretched premixed flames with imposed temperature profile (FlameMaster [42])

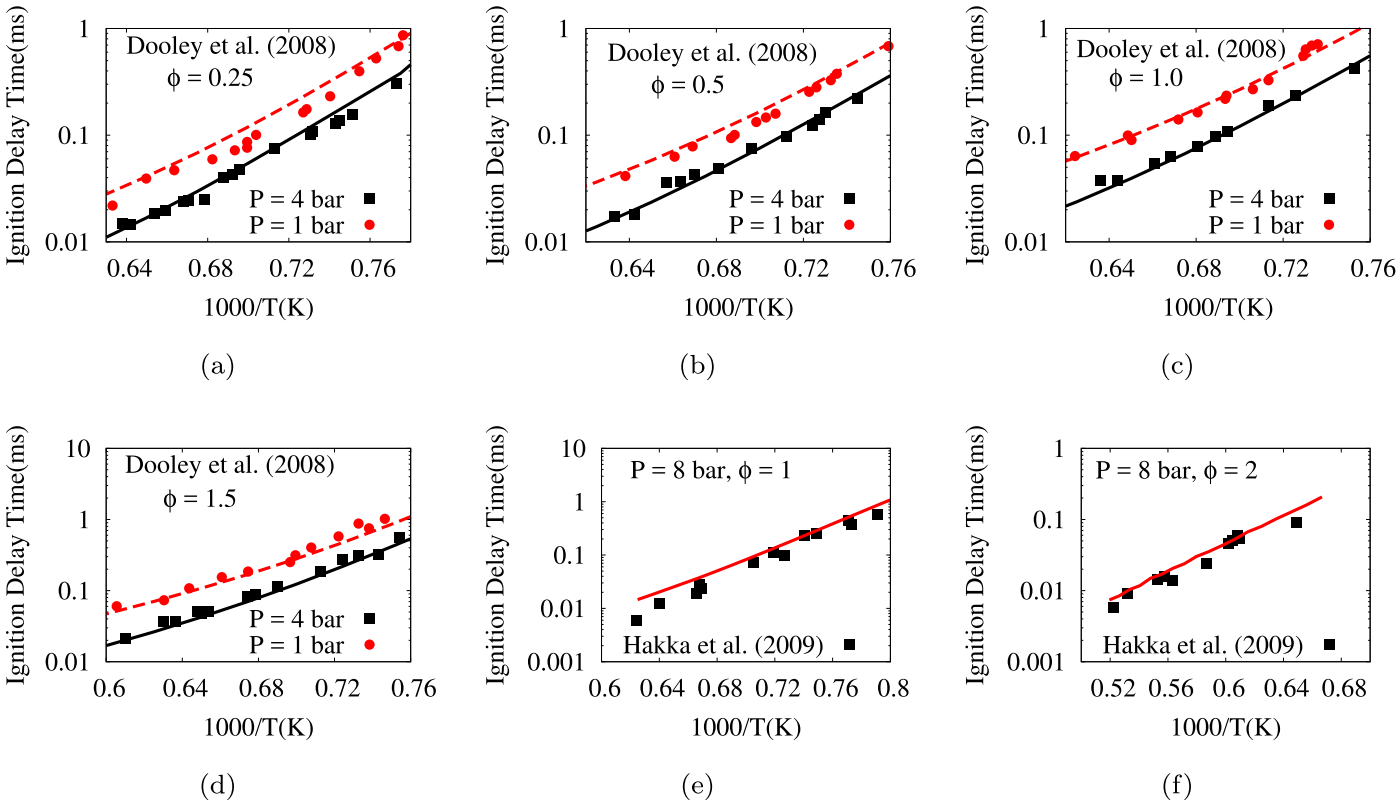

Fig. 8. Ignition delays of MB/O_2/diluent mixtures; symbols : experiments (Dooley et al. [11] (a)–(d) and Hakka et al. [15] (e), (f)); lines : simulations using the IITM high T model (solid and dashed lines correspond to square and circle symbols respectively). Ignition delay times are defined by the time required to reach 10% of the maximum OH concentration (a)–(d) and by the instant of maximum rate of rise in CH emission (e), (f). Symbols cover the uncertainties in the experiments.

4. Results and discussions

The IITM high T model described previously is comprehensively validated against a wide range of experiments here. These include (i) ignition delay time measurements in shock tubes and RCMs, (ii) species profile measurements in a jet stirred reactor (JSR) and variable pressure flow reactor (VPFR), (iii) laminar burning velocity measurements, and (iv) species concentrations in a counter-flow diffusion flame and a flat flame burner setup. Table 2 compiles a list of all the experimental data sets used for the validation.

The numerical calculations for shock tube, jet stirred reactor, laminar burning velocities, flat flame burner and counter-flow diffusion flames are carried out using the FlameMaster code (version 3.3.10, [42]). Table 3 lists the reactor configurations used to simulate these experiments. Simulations of the rapid compression machine studies are carried out using the volume profile method as discussed in Refs. [31,44]. Volume profiles generated from non-reactive pressure traces are used to account for the heat loss during and post compression. Volume-time history is generated using a non-reactive pressure signal for each operating condition using adiabatic relations and temperature dependent specific heat ratio values of the test mixture. Pressure signal simulated by using this volume profile matches exactly with the experimentally measured non-reactive pressure signal (see Fig. 7). The effect of heat loss captured by the computations is also reflected in the temperature profile shown in Fig. 7. Ignition delays are then computed in CHEMKIN-PRO [43] using a closed homogeneous reactor solver with the prescribed volume profile. Volume profiles for all the data points have been provided in the supplementary material.

4.1. Ignition delay time measurements

4.1.1. Shock tube

Simulated ignition delay times are compared here against shock tube experiments performed by Dooley et al. [11] and Hakka et al. [15] for MB/O_2/Ar mixtures. First, ignition delay times measured by Dooley et al. [11] over the temperature range 1250–1706 K at 1 and 4 atm and equivalence ratios of 0.25–1.5, are examined. Figure 8(a)–(d) show that the simulated ignition delay times are in excellent agreement with this dataset (within 15% for the most of the data points). Comparing against shock tube experiments of Hakka et al. [15] (see Fig. 8(e), (f)), it can be observed that the model displays good agreement with these experiments, except an overprediction at $\phi = 1$ and $T > 1600$ K. It can be concluded that

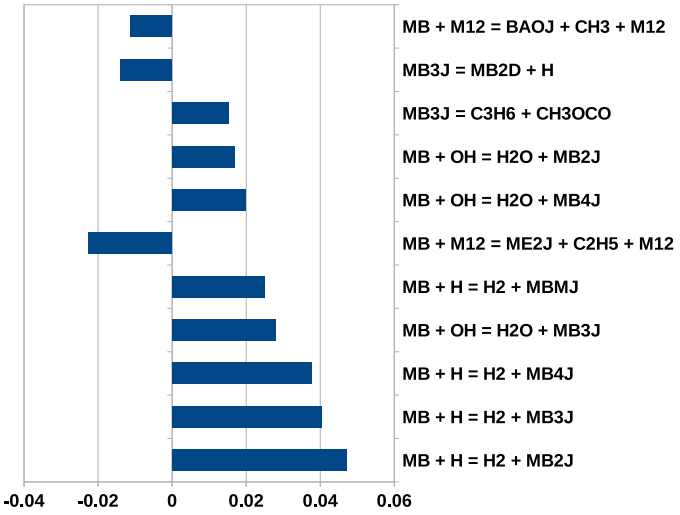

Fig. 9. Sensitivity analysis for ignition delays of MB/O_2/Ar mixtures at $\phi = 1.0$, $P = 4$ atm, and $T = 1300$ K. Sensitivities are determined by multiplying each rate constant by a factor of 2, and finding the corresponding change in ignition delays. Only those reactions involving fuel or fuel radicals with sensitivities ≥ 0.01 are reported here.

the mechanism successfully captures MB auto-ignition in the high temperature ($T > 1200$ K) regime.

A sensitivity analysis has been performed to identify pathways important for auto-ignition at high temperatures. Figure 9 summarizes the normalized sensitivity analysis for methyl butanoate specific reactions. Ignition delays are sensitive to H-atom abstraction by radicals, H and OH, from the fuel. Of these, the H-atom abstraction by H atoms at the site adjacent to the carbonyl C is vital, since this is the most favoured channel for this class of reactions. The reaction forming C_2H_5 has more effect on ignition delays than the one forming CH_3, since C_2H_5 from methyl butanoate would further give rise to an H-atom. Also, H-atom formation from MB3J will accelerate the overall reaction progress and would result in shorter ignition delays. An integrated path flux analysis performed at same conditions reveals that 40% of the fuel is consumed through H-atom abstraction by H-atoms, 18% through fuel decomposition, and the rest is H-atom abstraction reactions by other radicals, predominantly OH and O. Updated rates for H-atom abstraction from the fuel by H-atoms, fuel decomposition, and the use of a well validated base chemistry in our model result in good agreement of the computed ignition delays with the experiments, as presented above.

4.1.2. Rapid compression machine

Ignition delays measured in RCMs provide us valuable data for the evaluation of kinetic description in low to intermediate temperature regimes for fuels having longer ignition delays (5–200 ms). They are often influenced by the effects of heat loss, turbulence fluctuations, and temperature inhomogeneities [49,50]. Attempts have been made to capture the non-idealities in RCM experiments by performing CFD simulations with detailed chemistry [50], but such a computationally extensive effort is beyond the scope of this study. Thus, the effect of heat loss alone has been accounted for in our simulations as discussed earlier in this section. The importance of the remaining uncertainties is discussed below while interpreting our results.

In the present work, ignition delay times are measured in an rapid compression machine at varied pressures, temperatures and equivalence ratios, allowing a thorough assessment of the auto-ignition characteristics of the MB kinetic mechanism in the intermediate temperature range as well. Also, for the first time, ignition delays have been measured for rich mixtures in this temperature range, providing additional data-sets for validating chemical

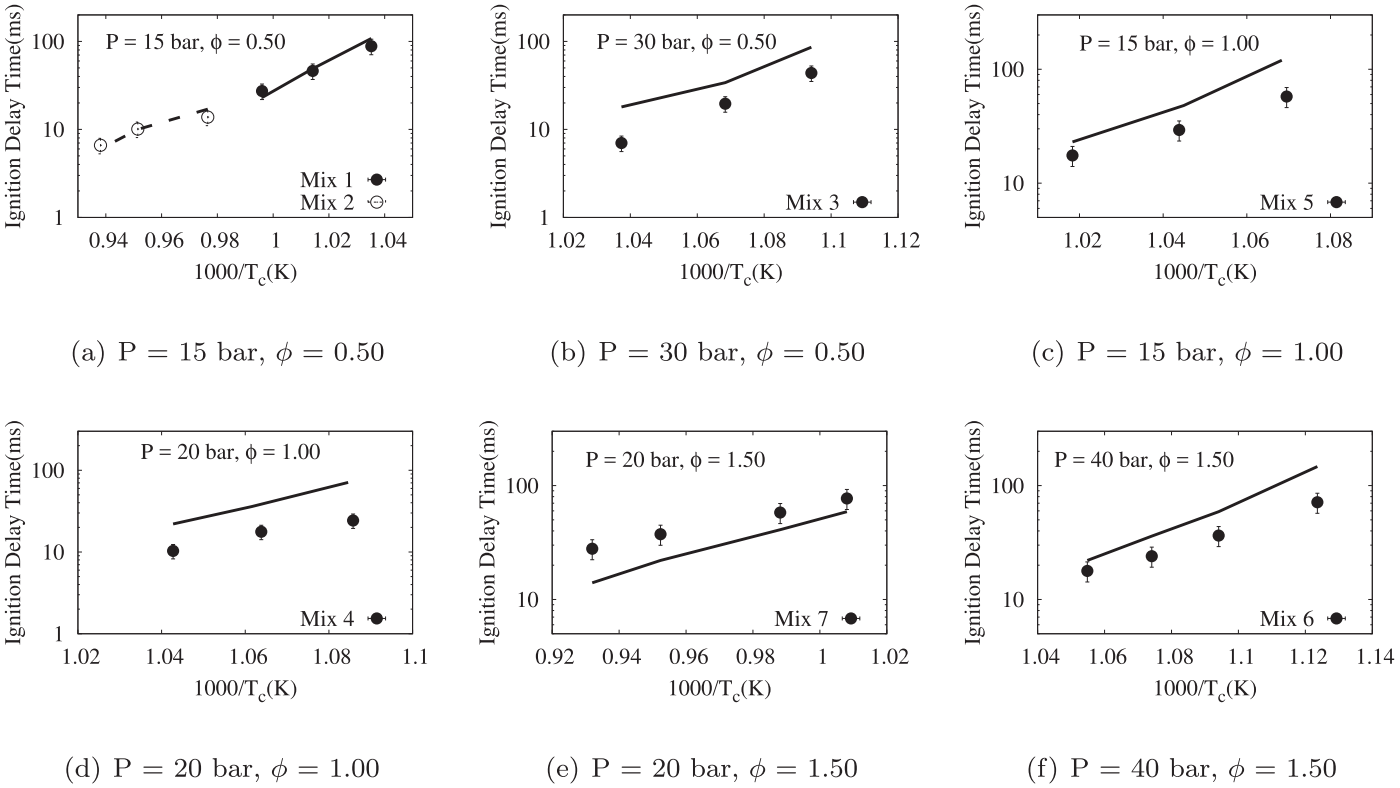

Fig. 10. Ignition delays of MB/O_2/diluent mixtures; symbols : experiments from this study; lines: simulations. Ignition delays are defined based on the time required for maximum rate of pressure rise in the experiments and the same criterion is used in the simulations as well.

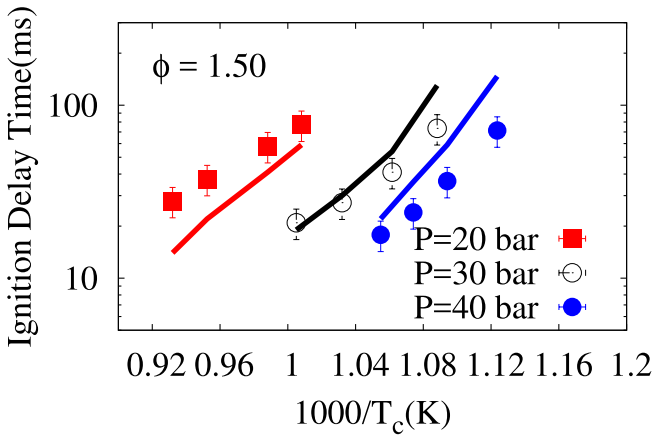

(a) P = 20 bar, P = 30 bar and P = 40 bar

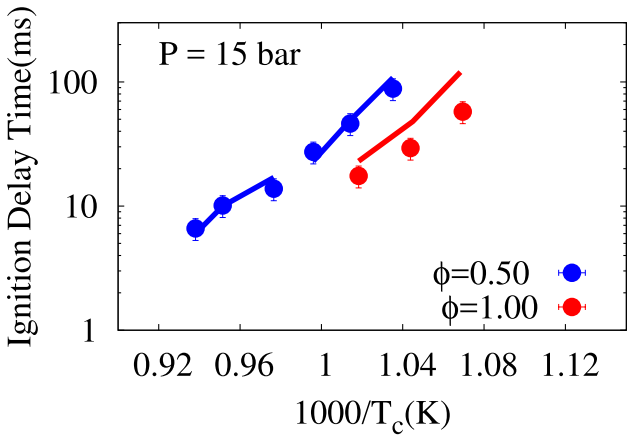

(b) ϕ = 0.50 and ϕ= 1.00

Fig. 11. Effect of (a) pressure and (b) equivalence ratio on ignition delays; symbols : experiments (this study); lines: simulations. The experimental dataset is same as that presented in Fig. 10, re-plotted to bring out the trends when varying pressure and equivalence ratios.

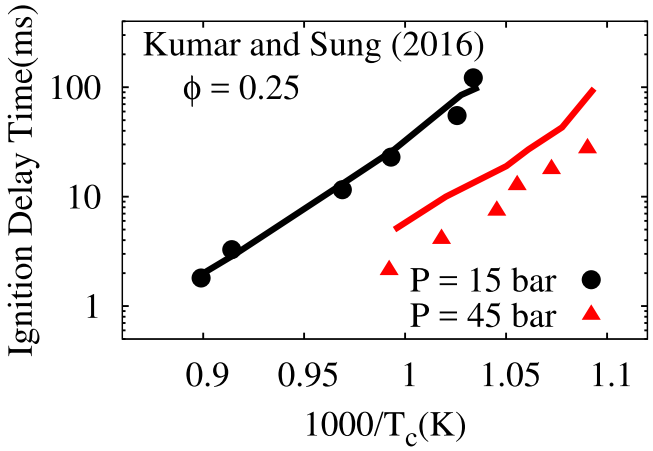

Fig. 12. Ignition delays of MB/O_2/Ar mixtures; symbols: experiments from Kumar and Sung [29]; lines: simulations. Ignition delays are defined based on the instant of maximum rate of pressure rise and and the same criterion is used in the simulations as well. Symbols cover the uncertainties in the experiments.

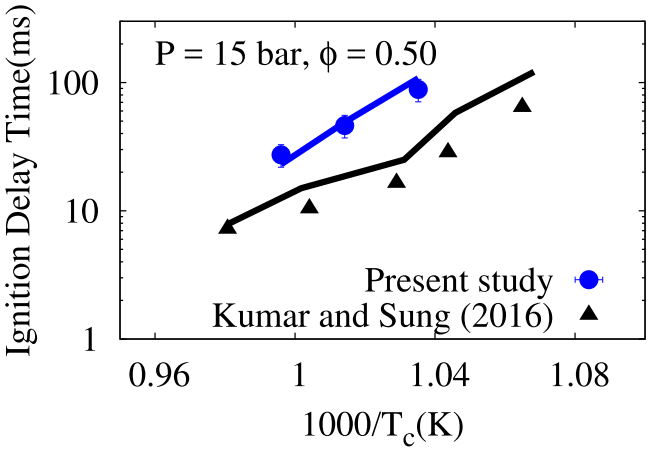

Fig. 13. Comparison between the ignition delays measured in this work and in Kumar and Sung [29] at similar conditions and the corresponding simulations.

kinetic models. It should be noted that although the temperature varies from the start of the experiment in an RCM to the end, the data has been plotted against T_c, which is the end of compression temperature, to conform to the recommended standard way of representing these data sets.

Figure 10 shows the comparison between the computed ignition delays against the experimental data. The model shows reasonable agreement with experiments, considering the uncertainties discussed above. Firstly, for lean mixtures, the kinetic model agrees well with the experiments at $P = 15$ bar (see Fig. 10(a)), but predicts longer ignition delays at higher pressures (see Fig. 10(b)). Similarly, longer ignition delays are predicted at stoichiometric conditions as shown in Fig. 10(c), (d). For rich mixtures, the model underpredicts the ignition delays at 20 bar while overpredicting them at higher pressures (see Figs. 10(e), (f)).

To further assess the reactivity of the kinetic model, the effects of pressure and equivalence ratios are considered in Fig. 11. As shown in Fig. 11(a), increasing the pressure increases the reactivity of the fuel, which is captured well by the model proposed here. The kinetic scheme shows relatively weaker dependence on pressure compared to that of the experiments. The model also captures the effect of change in equivalence ratio as seen from Fig. 11(b). Similar agreement has been found at other equivalence ratios as well (see supplementary materials, Fig. S4).

It can be concluded that the model shows satisfactory agreement with the experimental data considering the uncertainties in RCM experiments. However, the model is unable to capture the extent of the pressure dependency at these conditions. Those pressure dependent reactions that are important at these conditions and are a part of the base chemistry, have been derived from either theoretical studies or experimental investigations. Therefore, it seems appropriate to consider pressure dependence of the fuel submodel to capture this effect. For instance, an ab-initio study performed by Tan et al. [59] on methyl propanoate radicals suggests a pressure dependence in the intermediate and high temperature range (900–1600 K) for isomerization as well as decomposition reactions of the methyl propanoate radicals. An investigation on the pressure dependence of the corresponding reactions involving methyl butanoate radicals will be helpful to further improve the pressure dependence exhibited by the kinetic model.

Ignition delays of MB have also been measured in an RCM by Kumar and Sung [29]. Figure 12 compares the simulations performed using our kinetic model with these experiments. Similar to the trends shown in Figs. 10 and 11, the model shows good

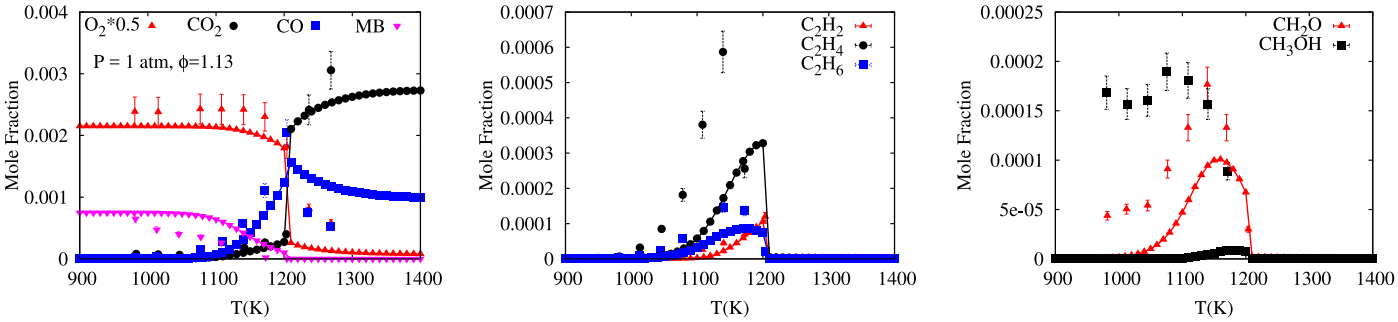

Fig. 14. Species concentrations versus initial temperature measured in a JSR at atmospheric condition for $\phi = 1.13$. Symbols: experimental data from Gail et al. [13]; lines with symbols: simulations.

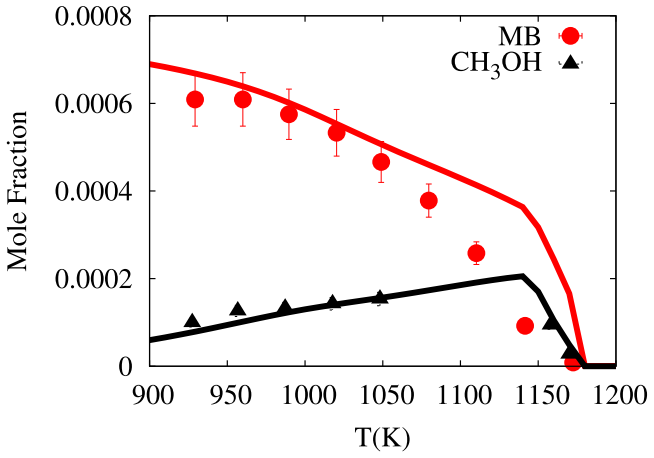

Fig. 15. Concentrations of methyl butanoate and methanol at $P = 1$ atm and $\phi = 0.75$ in a JSR. Symbols: experiments [13]; lines: results from simulations after addition of fuel decomposition pathway producing methanol to account for wall reactions.

agreement with the experiments for lean mixtures at 15 bar, but predicts longer ignition delays at higher pressures (see Fig. 12).

Note that even though the RCMs employed in the present work and Kumar and Sung [29] are identical in design, the initial conditions, mixture compositions and compression ratios used are different. These factors can lead to different extents of non-idealities as discussed earlier. Hence, even though the model captures the overall variation in ignition delays with Kumar and Sung [29] experimental data, the extent of agreement varies based on the experimental conditions.

To emphasize this further and bring out the facility effects, Fig. 13 shows a comparison between experimental data from Kumar and Sung [29] as well as the present work at 15 bar and $\phi = 0.50$ in the two different RCMs. This difference in measured ignition delays may be attributed to the different amounts of heat losses and extent of inhomogeneities manifested in the two set of experiments. The magnitude of heat loss is a function of mixture composition, compression ratio, operating conditions and machine dimensions. The use of similar machine dimensions in our experiments and those of Kumar and Sung [29] limits the difference in measured data to the remaining factors.

Simulations using the present IITM high T model shown in Fig. 13 capture this effect and follow the trend in experimental data. Note that the heat loss has been accounted for in the present simulations by imposing the volume profile generated during the non-reactive experiment. However, this volume profile still does not account for any local inhomogeneities occurring inside the combustion chamber as it is based on the measurement of overall pressure inside the combustion chamber. This can explain the differences shown by the simulations compared to the data sets at similar overall conditions. This again reiterates that RCM experiments should be interpreted carefully by considering the effects of non-idealities, as discussed previously.

The experimental data sets presented here have also been used to validate several existing detailed mechanisms for methyl butanoate [11,13,15] (not shown here). All the models predict consistently shorter ignition delays by a factor of 2–4 as compared to the RCM ignition delay time experiments presented in this work, similar to the conclusions drawn by Kumar and Sung [29]. This difference can be attributed to the rate constants employed for reactions important to the oxidation of methyl butanoate at conditions explored in the RCM. In the existing models, the rate parameters are derived from analogous reactions among alkanes, whereas the model proposed here benefits from the recent theoretical investigations of methyl butanoate kinetics as discussed earlier.

4.2. Species concentration measurements

4.2.1. Jet stirred reactors

Gail et al. [13] studied the isothermal oxidation of methyl butanoate in a jet stirred reactor at atmospheric conditions and different equivalence ratios as a function of initial temperature. Figure 14 shows a comparison between the experimentally measured species profiles and the computations performed with our model at $P = 1$ atm and $\phi = 1.13$. The model shows good qualitative agreement with the experiments. Among the major species, fuel (MB) consumption and CO production is underestimated by the model, while among the trace species, model severely underpredicts the concentration of methanol. Similar results were obtained at other equivalence ratios as well.

It has been found that our proposed model cannot be modified to account for the extent of methanol production shown by experiments without affecting the agreement with other species. This was also considered in Dooley et al. [11] and they proposed the addition of pathways for wall reaction resulting in methanol production from fuel to explain the disagreement between the experiments and the model as a result of probable heterogeneous catalysis of MB by Si-OH sites on the reactor surface. Upon adding pathways for fuel decomposition into methanol and its subsequent product species, the model shows better agreement with the fuel consumption (see Fig. 15). Similar observations were found for the computed results at other mixture compositions as well. These modifications had the least effect on the prediction of other species concentrations.

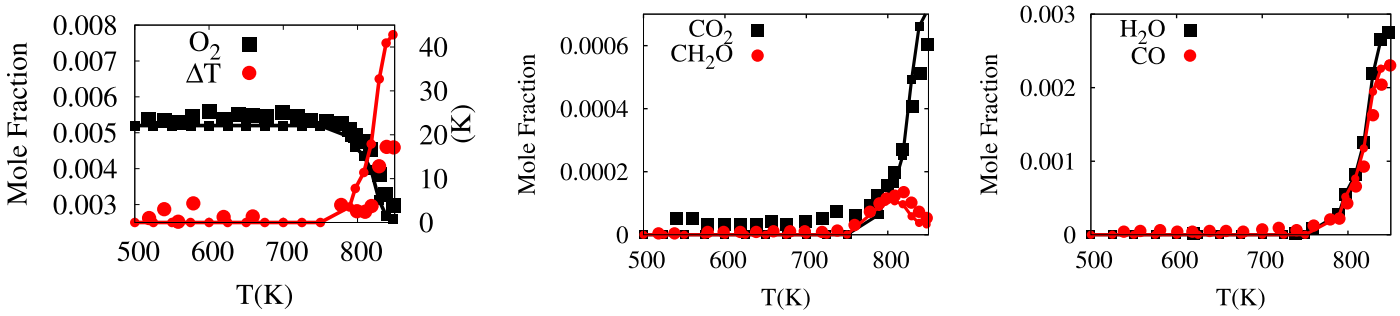

Fig. 16. Species concentrations versus initial temperature in Princeton VPFR at $P = 12.5$ atm and $\phi = 1$. Symbols : experiments from Marchese et al. [45]; lines with symbols : simulations.

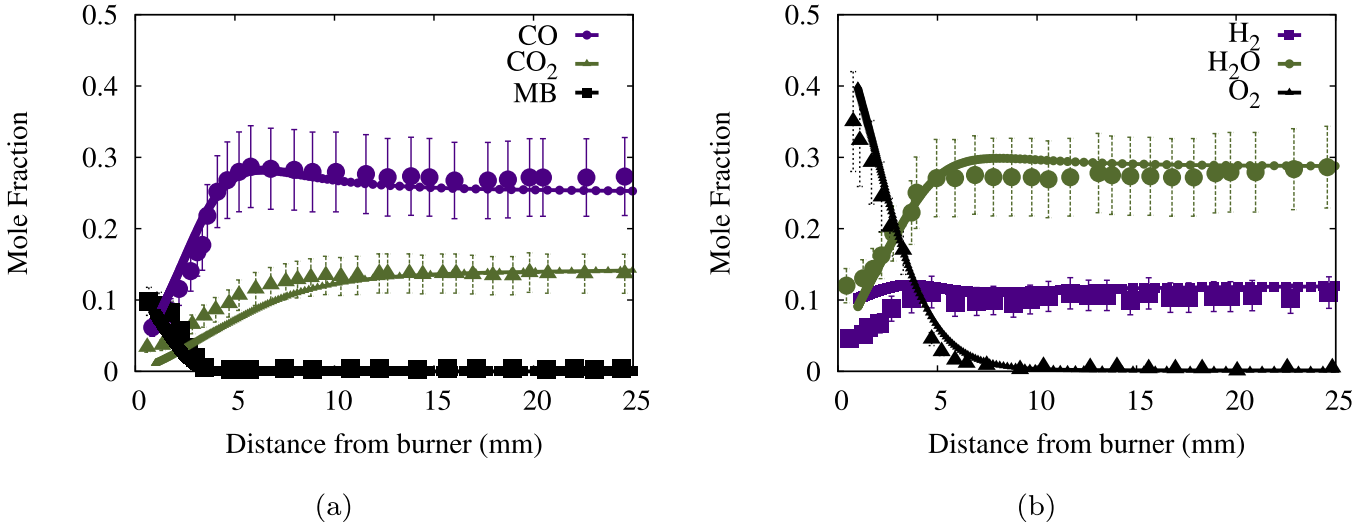

Fig. 17. Comparison between simulated and experimental species profiles for a premixed flat flame burner at $P = 30$ torr, $\phi = 1.56$; symbols: experiments by Yang et al. [46], lines with symbols: simulations with IITM high T model. Simulated species profiles have been shifted by 1 mm.

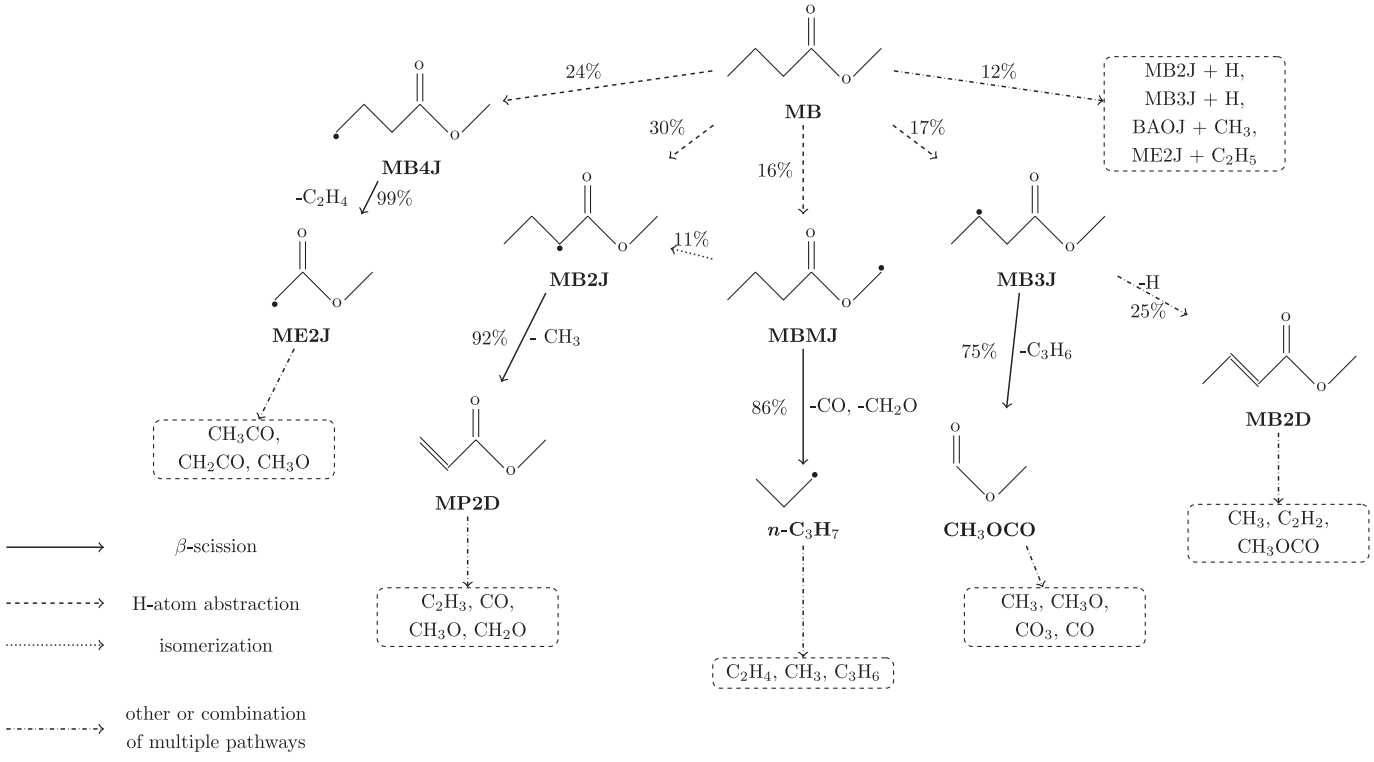

Fig. 18. Path flux analysis for methyl butanoate at conditions specified in Fig. 17.

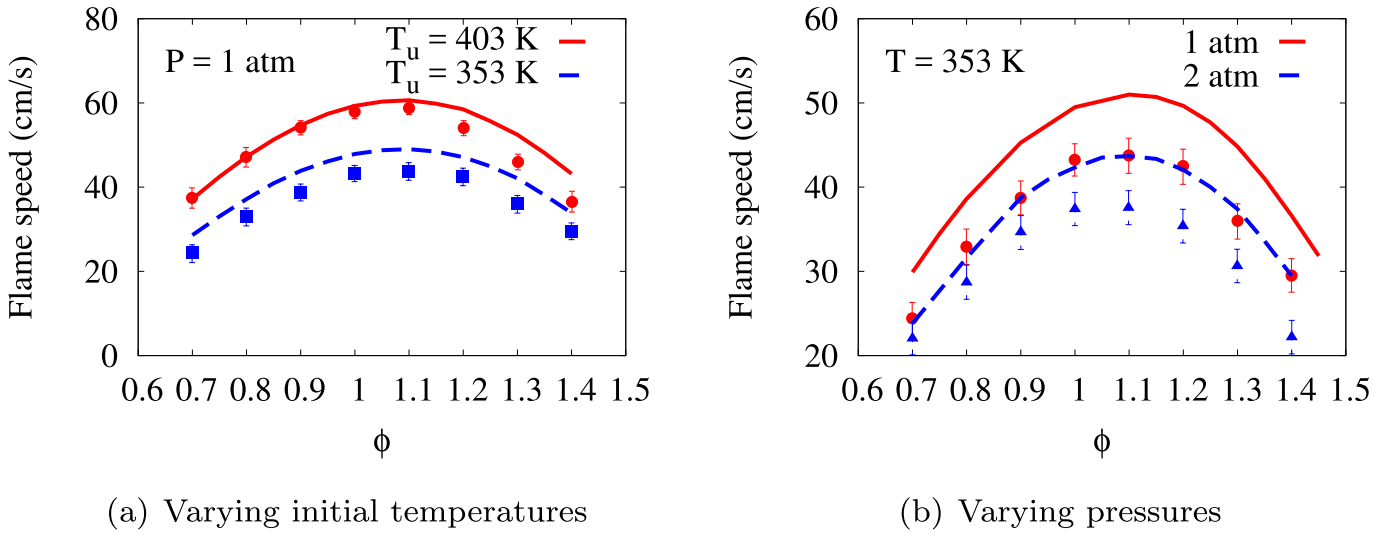

Fig. 19. Laminar burning velocities of MB/Air mixture as a function of equivalence ratio for (a) varying initial temperature, $T_u = 353$, 403 K and $P = 1$ atm, and (b) varying pressure at initial $T = 353$ K; symbols: Experiments from Wang et al. [37] (403 K) and Liu et al. [47] (353 K); lines: simulations performed using the IITM high T model.

4.2.2. Variable pressure flow reactor

Reactivity experiments were conducted in the Princeton VPFR by Marchese et al. [45] at 12.5 atm, $\phi = 0.35$, 1, 1.50 and $T = 500$–900 K using methyl butanoate as the fuel. Species concentrations were reported as a function of initial temperature at a fixed residence time of 1.8 s. These chemical reactivity experiments are simulated in the present work by employing a time-shifting procedure as suggested in Jahagirian et al. [51]. The time shifting required at each temperature is determined by matching the concentration of H_2O measured in the experiments, since species-time histories have not been reported for methyl butanoate. Thus, the time shifting employed depends on the initial temperature as well as the kinetic model [51].

Although spanning a temperature range of 500–900 K, no NTC behavior was reported. Hence, IITM high T model, which has been used to carry out all the simulations till the present section is also appropriate to model these experiments. Figure 16 compares the computations performed using the IITM high T model at $\phi = 1$ with the experiments. Time shifts in the range of 5–9 s were employed based on the initial reactor temperature. The model agrees well with the species concentrations reported by the experiments. Similar agreement has been found at lean and rich mixture ratios as well. Computations predict a higher heat release compared to the experiments (see Fig. 16) at lower initial temperatures. Computations have been performed here as an adiabatic homogeneous reactor and the disagreement may be attributed to any possible heat loss during the experiments that is not accounted for here. Nevertheless, this remains to be a favourable result at these moderate temperatures, considering the ability of the model to correctly predict the amount of CO and CO_2, which are closely related to the heat release.

4.3. Flame studies

4.3.1. Flat flame burner

Yang et al. [46] measured the amounts of reaction intermediates in low-pressure premixed flat flames at rich conditions. Figure 17 compares the computed species profiles with experiments as a function of distance away from the burner. Simulated species profiles have been shifted by 1 mm for better agreement with the experiments, which is within the uncertainties stated in the experimental study [46].

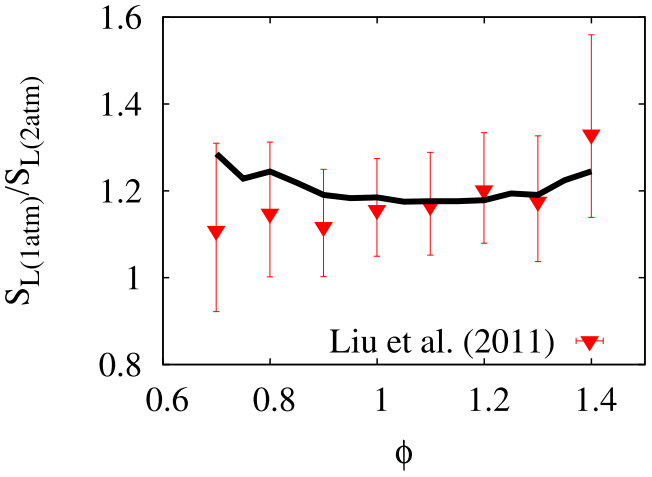

Fig. 20. Dependence of burning velocities on pressure. Symbols: experiments [47]; lines: simulations.

Figure 17 show that the simulated concentrations of major species show an excellent agreement with the experiments, except for H_2 concentration very near to the burner. This could be the result of larger uncertainties present very close to the burner [52]. Further, for minor species and oxygenates, the model is found to agree with the experiments well within the quoted uncertainties (see supplementary materials, Fig. S5). Overall, the model captures the concentrations of the major species as well as the reaction intermediates in these premixed flat flames.

A path flux analysis for fuel indicates that the majority of the fuel is consumed via H-atom abstraction from fuel by different radicals (see Fig. 18), predominantly by H, owing to the higher temperatures ($T > 1100$ K) in the flame region, where the fuel is consumed (see Fig. 17(a)). Again, MB2J radical is favoured over the other methyl butanoate radicals due to its resonantly stabilized structure (see Fig. 5). These fuel alkyl ester radicals, formed through H-atom abstraction pathways, primarily undergo β-scission reactions to form a range of oxygenated species such as smaller methyl ester radical (ME2J) and C_1–C_3 species. These smaller species and subsequent intermediates further react to form the major products.

4.3.2. Laminar burning velocities

Wang et al. [37] measured laminar burning velocities of MB/air mixture as a function of equivalence ratio under atmospheric conditions and a preheated temperature of 403 K in a counter-flow configuration. Liu et al. [47] also determined burning velocities of MB/air mixture as a function of equivalence ratio as well as pressure by using a heated dual-chambered combustion vessel at 353 K. Unstretched burning velocities are determined by non-linear extrapolation for both sets of experiments.

Figure 19 shows a comparison between the computed flame speeds and the experimental measurements. The model overpredicts the flame speeds compared to the experiments by 1–6 cm/s, despite showing improved results compared to the reference mechanism (see Figure 3). Flame speed predictions are sensitive to the reactions involving C_0–C_2 chemistry and H-atom abstraction from the fuel by H-atoms. The proposed model has been verified to show excellent agreement with experimental flame speed measurements for *n*-dodecane (see supplementary materials, Fig. S10(c)), which it is also valid for. Additionally, the base chemistry has also been successfully validated against flame speeds of smaller species. Hence, the onus appears to be on the rate constants used for the H-atom abstraction reactions by H-atoms to explain the disagreement with the flame speed measurements. Nevertheless, it should be noted that the model shows excellent agreement for high temperature auto-ignition, where this class of reactions is highly important. This suggests that additional experimental data are needed to conclusively decide about the ability of the proposed model to predict laminar flame speeds.

To investigate the pressure dependence separately, ratio of flame speeds measured at different pressures are compared with the simulations. Figure 20 shows that the flame speed ratio computed using model agrees well with the experiments, lending confidence to the kinetic description in our model.

5. Addition of low-temperature chemistry pathways

The reference methyl butanoate mechanism [11] used in this study does not include any reactions pertaining to the low-temperature chemistry. The low-temperature chemistry pathways, involving addition of O_2 to the fuel radical and the subsequent reactions, lead to the non-Arrhenius behaviour shown by several hydrocarbons at $T \sim 900$ K depending on the pressure and the type of the fuel (such as shown by Refs. [38,39]). This behavior can be characterized by a negative temperature co-efficient regime, where the ignition delays increase with increase in temperature. Several other indicators such as the presence of two stage heat release in RCM or the consumption of fuel in two stages in JSR can also reveal the presence of NTC regime and necessitates including low-temperature chemistry pathways to describe this combustion behavior.

Nevertheless, none of the experiments performed with methyl butanoate including the ignition delay time measurements presented in this study exhibit any NTC behavior or two-stage ignition. This indicates that the low-temperature chemistry pathways may not play an important role in the parameter (P, T, ϕ) space investigated in literature, which cover a wide range of conditions including those relevant for engine applications. Hence, including the low-temperature chemistry to MB kinetic description may not be crucial for conditions of interest here. Nevertheless, for the sake of investigating all aspects of MB kinetics across different operating conditions, which may be affected by the low-temperature chemistry, we have explored the addition of these pathways to the MB sub-mechanism.

The reaction of fuel radical (R) with O_2 molecule forming the peroxy radical (ROO) and its reverse is central to low-temperature chemistry [53]. The rates for this class of reactions are assigned here from a theoretical study on an analogous molecule, methyl propanoate [54]. The reactions of intramolecular H-migration in ROO, concerted elimination of ROO and QOOH, as well as reactions of ROO+HO_2 are taken from the recent theoretical study by Tao and Lin [23]. Their sub-mechanism presents rate parameters for 114 pathways along with the thermochemistry for the species involved. Since many of these pathways have potential energy barriers much higher than that of ROO $\longrightarrow$ R + O_2, pathways with energy barrier higher than 10 kcal/mol compared to the peroxy decomposition reaction are omitted to limit the number of additional reactions.

For the second O_2 addition to QOOH and the subsequent branching pathways, the rate constants are taken from Jiao et al. [22]. Their investigation at the G3MP2B3 level of theory indicated the importance of radical inter-conversion within OOQOOH radicals through 8–, 10– and 11–membered ring transition states along with its decomposition reactions. Reactions for these radicals were not considered significant because of the size of the transition state rings involved. The activation energies for decomposition of keto-hydroperoxide formed during low-temperature branching have also been derived from this study.

In summary, the above sets of reactions include the most significant reaction classes deemed important for low-temperature autoignition. Rate constants have been assigned for pathways among species derived from the above reaction sets from similar studies of other hydrocarbons [14,41] to ensure their consistent representation, whose values were not given as a part of the investigation in Refs. [22,23]. This has resulted in consideration of 18 reaction classes comprising of 250 reactions in the low-temperature sub-mechanism. Table 4 summarizes these additional reaction classes. Effects of addition of these reactions to the 'IITM high T model' are discussed below. The full model including low-temperature pathways as well as the corresponding thermodynamic and transport data files are made available with the supplementary materials along with the species nomenclature.

Effect of adding low-temperature pathways

As discussed earlier, the auto-ignition of MB at low temperatures (< 800 K) is strongly dependent on the HO_2 radical. The concerted elimination of ROO radicals is a principal contributor of HO_2 radicals. Rate constants for this reaction class were determined by Tao and Lin [23] and Jiao et al. [22] by employing MP2B3 and CBS-QB3 levels of theory, respectively. Incorporating the rate constants at the CBS-QB3 level in the model results in an NTC behavior at the conditions of the RCM experiments performed in this study, while no such phenomena is exhibited in the experiments. Adopting the rate constants at the MP2B3 level of theory results in slower reactivity compared to the experiments without any NTC behavior. Path flux analysis at $P = 40$ bar, $\phi = 1$ and $T = 900$ K reveals that 90% of the fuel-peroxy radical is consumed through the concerted elimination pathway when rate constants are prescribed at the MP2B3 level of theory resulting in reduced reactivity, while only 60% is consumed through the same with rate constants obtained at the CBS-QB3 level of theory, thereby resulting in NTC behavior due to production of sufficient amounts of QOOH radicals.

In view of these discrepancies, in the present model, the rate constants for the concerted elimination pathways have been reduced by a factor of 3 from the values calculated at the MP2B3 theory, to ensure that the proposed model confirms with the absence of any low-temperature behavior displayed in the auto-ignition experiments presented in this study. Figure 21 compares the computed results for some representative cases of auto-ignition experiments. The results obtained for ignition delay times using the complete model that includes the low-temperature path-

Table 4
Summery of additional pathways incorporated in the IITM high T model as a part of the low-temperature chemistry.

Reaction class	Source	Comments
$R + O_2 \longrightarrow RO_2$	Le et al. [54]	Analogy with Methyl propanoate. For O_2 addition to γ-C in methyl butanoate assigned rates based on average of rates for O_2 addition to β-C and γ-C in methyl propanoate
$RO_2 \longrightarrow QOOH$	Tao et al. [23]	G3MP2B3 composite approach
$RO_2 \longrightarrow$ alkene + HO_2	Tao et al. [23]	G3MP2B3 composite approach. Rates modified as explained in the main article.
$RO_2 + HO_2 \longrightarrow ROOH + O_2$	Tao et al. [23]	G3MP2B3 composite approach
$ROOH \longrightarrow RO + OH$	Sarathy et al. [55]	Based on analogy with alkanes
$R + ROO \longrightarrow RO + RO$		
$R + HO_2 \longrightarrow RO + OH$		
$R + CH_3O_2 \longrightarrow RO + CH_3O$		
$ROO + H_2O_2 \longrightarrow ROOH + HO_2$		
$ROO + CH_3O_2 \longrightarrow RO + CH_3O + O_2$		
$ROO + ROO \longrightarrow RO + RO + O_2$		
$QOOH \longrightarrow$ alkene + HO_2	Tao et al. [23]	G3MP2B3 composite approach
$QOOH \longrightarrow$ cyclic ether + OH	Tao et al. [23]	G3MP2B3 composite approach
Reactions of cyclic ethers	Dievart et al. [14]	Based on analogy with alkanes
$QOOH + O_2 \longrightarrow O_2QOOH$	Le et al. [54]	Analogy with Methyl propanoate. For O_2 addition to γ-C in methyl butanoate assigned rates based on average of rates for O_2 addition to β-C and γ-C in methyl propanoate
O_2QOOH isomerization	Jiao et al. [22]	CBS - QB3 calculations
$O_2QOOH \longrightarrow$ alkenyl ester peroxy + HO_2		
$O_2QOOH \longrightarrow$ KET + OH		
KET decomposition	Dievart et al. [14]	Based on analogy with alkanes. Activation energies modified based on Jiao et al. [22] study.

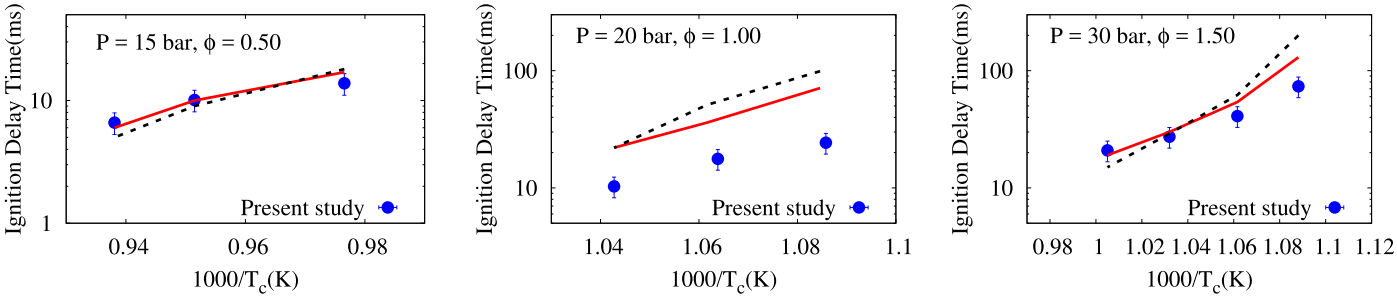

Fig. 21. Ignition delay time measurements for MB/O_2/diluent mixtures in an RCM. symbols : experiments (present study), lines: Simulations – IITM high T model (solid lines), IITM MB model that includes additional low-temperature pathways as well (dashed lines).

ways are similar to those obtained from the IITM high T model. Similar conclusions can be drawn for JSR and VPFR configurations as well (see supplementary materials, Figs. S7 and S8). These comparisons have to be viewed with caution, since the modifications introduced here to the rate constants of the concerted elimination pathways can be justified only if the model can predict the low temperature oxidation behavior of methyl butanoate accurately.

Hence, this discussion leads to the following conclusions: (i) The addition of low-temperature pathways do not make much difference to the results presented here, suggesting that the low-temperature pathways are not important for the the parameter (P, T, ϕ) space investigated in the MB experiments presented in the literature or in the present work. (ii) However, the present model does suggest the occurrence of NTC at 60 bar for stoichiometric mixtures for a temperature range of 850–890 K (see supplementary materials, Fig. S9). (iii) Additional experiments are required in these proposed operating conditions to correctly assess the low-temperature chemistry for MB. The low-temperature chemistry submodel proposed here needs to be revisited once the additional experimental data is available. In summary, although the addition of low-temperature pathways is not found to play a role at (P, T, ϕ) conditions presented in this work, it can become important at other conditions (such as the one suggested above). Further, an accurate kinetic description of low-temperature chemistry for the small ester, methyl butanoate, can also be used to propose rate rules for these reaction classes for longer esters, which have not been investigated thoroughly by theoretical calculations or experiments.

6. Conclusions

A compact kinetic mechanism has been developed for methyl butanoate, which is a suitable candidate to represent the ester content in biodiesel surrogates. A detailed reaction mechanism for methyl butanoate (Dooley et al., 2008) has been reduced using DRGEP technique [34] and combined in a consistent manner with a well validated *n*-dodecane model (Narayanaswamy et al., 2014), in view of the potential of this long chain alkane along with methyl butanoate as a component of biodiesel surrogate. The resulting model is comprehensively assessed for methyl butanoate kinetic. Several changes have been incorporated in the rate constants of the important reaction classes in methyl butanoate oxidation prompted by recommendations from recent theoretical investigations. The MB submodel is now based on rate parameters drawn from theoretical calculations wherever available. The resulting mechanism has been comprehensively assessed for methyl butanoate oxidation in various configurations including ignition delay times in shock tubes and RCMs, species profiles in JSR and VPFR, laminar burning velocities and species profiles in flat flame burner and counter-flow diffusion flames. The proposed model has been found to satisfactorily predict these data-sets. Addition of low-temperature chemistry pathways has also been explored and the need for additional experiments to assess the rate constants assigned to reactions important at these temperatures has been identified.

As a part of the present work, the experimental data in literature have been complemented by additional ignition delay time measurements in rapid compression machines. No NTC or two

stage ignition behavior was observed in these autoignition experiments. This experimental data along with the volume profiles required to simulate RCM ignition delay time experiments have been made available as a part of the supplementary materials.

It is worth re-emphasizing the salient contributions of the present work: (i) a compact skeletal kinetic model for methyl butanoate kinetics has been developed. (ii) This kinetic scheme has been well validated for a variety of experimental data and shows better predictions for RCM ignition delay time measurements and flame speeds compared to existing methyl butanoate oxidation models proposed in the literature [11,13,14], while retaining the agreement with other configurations including shock tubes, jet stirred reactor, variable pressure flow reactor and flat flame burner. (iii) Ignition delay time data for rich mixtures have been reported for the first time in the intermediate temperature range (800–1000 K), which serves as a useful validation target for future kinetic models as well and, (iv) low-temperature oxidation of methyl butanoate has also been explored, which proposes a potential pressure-temperature range for experimental investigation to correctly assess the low-temperature chemistry for MB.

Developed by extending an existing *n*-dodecane model [30] to describe the oxidation of methyl butanoate with good fidelity, this combined kinetic model has also been verified to predict *n*-dodecane kinetics accurately. Assessing the suitability of methyl butanoate and *n*-dodecane as a biodiesel surrogate will be taken up as a part of our future work. The models described here, with and without the additional low-tempera ture chemistry pathways, along with the corresponding thermodynamic and transport properties have been made available as Supporting Materials along with the nomenclature for MB sub-mechanism.

Acknowledgments

This material is based upon work supported as a part of the innoINDIGO BiofCFD project. The authors like to thank Dr. Perrine Pepiot from Cornell University for sharing the source code for DRGEP technique and the mechanism combination tool. The authors acknowledge support from the National Center for Combustion Research and Development (NCCRD), India for providing access to CHEMKIN-PRO software. The last author gratefully acknowledges support from the New Faculty Initiation Grant, Project no. MEE/15–16/845/NFIG offered by the Indian Institute of Technology Madras. The first author acknowledges the support provided by Indo-German centre for sustainability (IGCS) for an internship to perform RCM experiments at PTB, Germany. Valuable discussions with Prof. Frederick Dryer from Princeton University regarding VPFR simulations and inputs from Dr. Malcolm Lawes from University of Leeds about uncertainties in RCM facilities are also greatfully acknowledged.

Supplementary material

Supplementary material associated with this article can be found, in the online version, at 10.1016/j.combustflame.2018.06.033.

References

[1] K. Anand, R.P. Sharma, P.S. Mehta, Experimental investigations on combustion of jatropha methyl ester in a turbocharged direct-injection diesel engine, P. I. Mech. Eng. D J Aut. Eng. 222 (2008) 1865–1877.
[2] A. Demirbas, Progress and recent trends in biodiesel fuels, Energ. Convers. Manag. 50 (2009) 14–34.
[3] C.K. Westbrook, C.V. Naik, O. Herbinet, W. Pitz, M. Mehl, S.M. Sarathy, H.J. Curran, Detailed chemical kinetic reaction mechanisms for soy and rapeseed biodiesel fuels, Combust. Flame 158 (2011) 742–755.
[4] P. Dagaut, S. Gail, M. Sahasrabudhe, Rapeseed oil methyl ester oxidation over extended ranges of pressure, temperature, equivalence ratio: experimental and modeling kinetic study, Proc. Combust. Inst. 31 (2007) 2955–2961.
[5] J.L. Brakora, Y. Ra, R.D. Reitz, J. McFarlane, C.S. Daw, Development and validation of a reduced reaction mechanism for biodiesel-fueled engine simulations, SAE Int. J. Fuels Lub. 1 (2008) 675–702. 2008-01-1378
[6] H.M. Ismail, H.K. Ng, S. Gan, T. Lucchini, A. Onorati, Development of a reduced biodiesel combustion kinetics mechanism for CFD modelling of a light-duty diesel engine, Fuel 106 (2013) 388–400.
[7] T. Liu, E. Jiaqiang, W. Yang, A. Hui, H. Cai, Development of a skeletal mechanism for biodiesel blend surrogates with varying fatty acid methyl esters proportion, Appl. Energy 162 (2016) 278–288.
[8] H. An, W.M. Yang, A. Maghbouli, J. Li, K.J. Chua, A skeletal mechanism for biodiesel blend surrogates combustion, Energ. Convers. Manag. 81 (2014) 51–59.
[9] Z. Luo, T. Lu, M.J. Maciaszek, S. Som, D.E. Longman, A reduced mechanism for high-temperature oxidation of biodiesel surrogates, Energ. Fuel 24 (2010) 6283–6293.
[10] A.D. Lele, K. Anand, K. Narayanaswamy, Surrogates for biodiesel: review and challenges, in: A. Agarwal, R. Agarwal, T. Gupta, B. Gurjar (Eds.), Biofuels, Springer, Singapore (2017), pp. 177–199. Biofuels, Green Energy and Technology
[11] S. Dooley, H.J. Curran, J.M. Simmie, Autoignition measurements and a validated kinetic model for the biodiesel surrogate, methyl butanoate, Combust. Flame 153 (2008) 2–32.
[12] E.M. Fisher, W.J. Pitz, H.J. Curran, C.K. Westbrook, Detailed chemical kinetic mechanisms for combustion of oxygenated fuels, Proc. Combust. Inst. 28 (2000) 1579–1586.
[13] S. Gaïl, S.M. Sarathy, M.J. Thomson, P. Diévart, P. Dagaut, Experimental and chemical kinetic modeling study of small methyl esters oxidation: methyl (e)-2-butenoate and methyl butanoate, Combust. Flame 155 (2008) 635–650.
[14] P. Diévart, S.H. Won, J. Gong, S. Dooley, Y. Ju, A comparative study of the chemical kinetic characteristics of small methyl esters in diffusion flame extinction, Proc. Combust. Inst. 34 (2013) 821–829.
[15] M.H. Hakka, H. Bennadji, J. Biet, M. Yahyaoui, B. Sirjean, V. Warth, L. Coniglio, O. Herbinet, P.A. Glaude, F. Billaud, F. Battin-Leclerc, Oxidation of methyl and ethyl butanoates, Int. J. Chem. Kinet. 42 (2010) 226–252. 2010
[16] S. Gaïl, M.J. Thomson, S.M. Sarathy, S.A. Syed, P. Dagaut, P. Diévart, A.J. Marchese, F.L. Dryer, A wide-ranging kinetic modeling study of methyl butanoate combustion, Proc. Combust. Inst. 31 (2007) 305–311.
[17] F. Battin-Leclerc, J. Biet, R. Bounaceur, G.M. Côme, R. Fournet, P.A. Glaude, X. Grandmougin, O. Herbinet, G. Scacchi, V. Warth, EXGAS-ALKANES-ESTERS: A software for the automatic generation of mechanisms for the oxidation of alkanes and esters, LRGP, UPR CNRS 3349 (2010).
[18] L.K. Huynh, A. Violi, Thermal decomposition of methyl butanoate: ab initio study of a biodiesel fuel surrogate, J. Org. Chem. 73 (2008) 94–101.
[19] W. Liu, R. Sivaramakrishnan, M.J. Davis, S. Som, D.E. Longman, T.F. Lu, Development of a reduced biodiesel surrogate model for compression ignition engine modeling, Proc. Combust. Inst 34 (2013) 401–409.
[20] J. Mendes, C.W. Zhou, H.J. Curran, Theoretical and kinetic study of the hydrogen atom abstraction reactions of esters with h2 radicals, J. Phys. Chem. A 117 (2013) 14006–14018.
[21] J. Mendes, C.W. Zhou, H.J. Curran, Theoretical study of the rate constants for the hydrogen atom abstraction reactions of esters with OH radicals, J. Phys. Chem. A 118 (2014) 4889–4899.
[22] Y. Jiao, F. Zhang, T.S. Dibble, Quantum chemical study of autoignition of methyl butanoate, J. Phys. Chem. A 119 (2015) 7282–7292.
[23] H. Tao, K.C. Lin, Pathways, kinetics and thermochemistry of methyl-ester peroxy radical decomposition in the low-temperature oxidation of methyl butanoate: a computational study of a biodiesel fuel surrogate, Combust. Flame 161 (2014) 2270–2287.
[24] B. Akih-Kumgeh, J.M. Bergthorson, Structure-reactivity trends of c1–c4 alkanoic acid methyl esters, Combust. Flame 158 (2011) 1037–1048.
[25] L.K. Huynh, K.C. Lin, A. Violi, Kinetic modeling of methyl butanoate in shock tube, J. Phys. Chem. A 112 (2008) 13470–13480.
[26] L. Zhang, Q. Chen, P. Zhang, A theoretical kinetics study of the reactions of methylbutanoate with hydrogen and hydroxyl radicals, Proc. Combust. Inst. 35 (2015) 481–489.
[27] K. HadjAli, M. Crochet, G. Vanhove, M. Ribaucour, R. Minetti, A study of the low temperature autoignition of methyl esters, Proc. Combust. Inst. 32 (2009) 239–246.
[28] S.M. Walton, M.S. Wooldridge, C.K. Westbrook, An experimental investigation of structural effects on the auto-ignition properties of two C5 esters, Proc. Combust. Inst. 32 (2009) 255–262.
[29] K. Kumar, C.J. Sung, Autoignition of methyl butanoate under engine relevant conditions, Combust. Flame 171 (2016) 1–14.
[30] K. Narayanaswamy, P. Pepiot, H. Pitsch, A chemical mechanism for low to high temperature oxidation of n-dodecane as a component of transportation fuel surrogates, Combust. Flame 161 (2014) 866–884.
[31] G. Mittal, C.J. Sung, A rapid compression machine for chemical kinetics studies at elevated pressures and temperatures, Combust. Sci. Technol. 179 (2007) 497–530.
[32] C. Morely. A chemical equilibrium package for windows 2004. Available from: http://www.gaseq.co.uk.
[33] B.W. Weber, C.J. Sung, UConnRCMPy: python-based data analysis for rapid compression machines, 2017. arXiv:1706.01984.
[34] P. Pepiot-Desjardins, H. Pitsch, An efficient error-propagation-based reduction method for large chemical kinetic mechanisms, Combust. Flame 154 (2008) 67–81.

[35] P. Pepiot-Desjardins, Automatic strategies for chemical mechanism reduction, Department of Mechanical Engineering, Stanford University, 2008 Ph.D. thesis.
[36] G. Blanquart, P. Pepiot-Desjardins, H. Pitsch, Chemical mechanism for high temperature combustion of engine relevant fuels with emphasis on soot precursors, Combust. Flame 156 (2009) 588–607.
[37] Y.L. Wang, Q. Feng, F.N. Egolfopoulos, T.T. Tsotsis, Studies of C_4 and C_{10} methyl ester flames, Combust. Flame 158 (2011) 1507–1519.
[38] H.J. Curran, P. Gaffuri, W.J. Pitz, C.K. Westbrook, A comprehensive modeling study of n-heptane oxidation, Combust. Flame 114 (1998) 149–177.
[39] H.J. Curran, P. Gaffuri, W.J. Pitz, C.K. Westbrook, A comprehensive modeling study of iso-octane oxidation, Combust. Flame 129 (2002) 253–280.
[40] C.K. Westbrook, Chemical kinetics of hydrocarbon ignition in practical combustion systems, Proc. Combust. Inst. 28 (2000) 1563–1577.
[41] S.M. Sarathy, S. Vranckx, K. Yasunaga, M. Mehl, P. Oßwald, W.K. Metcalfe, C.K. Westbrook, W.J. Pitz, K. Kohse-Höinghaus, R.X. Fernandes, H.J. Curran, A comprehensive chemical kinetic combustion model for the four butanol isomers, Combust. Flame 159 (2012) 2028–2055.
[42] H. Pitsch, M. Bollig, Flamemaster, a computer code for homogeneous and one-dimensional laminar flame calculations, Institut fur Technische Mechanik, RWTH Aachen, 1993 Master's thesis.
[43] R. CHEMKIN-PRO, Reaction design, Inc., San Diego, CA, 2011. 15112.
[44] B.W. Weber, C.J. Sung, Comparative autoignition trends in butanol isomers at elevated pressure, Energy Fuel 27 (2013) 1688–1698.
[45] A.J. Marchese, M. Angioletti, F.L. Dryer, Flow reactor studies of surrogate biodiesel fuels, 30th International Symposium on Combustion (2004), pp. 25–30.
[46] B. Yang, C.K. Westbrook, T.A. Cool, N. Hansen, K. Kohse-Höinghaus, Fuel-specific influences on the composition of reaction intermediates in premixed flames of three $c_5h_{10}o_2$ ester isomers, Phys. Chem. Chem. Phys. 13 (2011) 6901–6913.
[47] W. Liu, A.P. Kelley, C.K. Law, Non-premixed ignition, laminar flame propagation, and mechanism reduction of n-butanol, iso-butanol, and methyl butanoate, Proc. Combust. Inst. 33 (2011) 995–1002.
[48] K.P. Grogan, S.S. Goldsborough, M. Ihme, Ignition regimes in rapid compression machines, Combust. Flame 162 (2015) 3071–3080.
[49] D. Bradley, M. Lawes, M. Materego, Interpretation of auto-ignition delay times measured in different rapid compression machines, 25th International Colloquium on the Dynamics of Explosions and Reactive systems, Leeds (2015).
[50] G. Mittal, M.P. Raju, C.J. Sung, Computational fluid dynamics modeling of hydrogen ignition in a rapid compression machine, Combust. Flame 155 (2008) 417–428.
[51] S. Jahangirian, S. Dooley, F.M. Haas, F.L. Dryer, A detailed experimental and kinetic modeling study of n-decane oxidation at elevated pressures, Combust. Flame 159 (2012) 30–43.
[52] U. Struckmeier, P. Oßwald, T. Kasper, L. Böhling, M. Heusing, M. Köhler, A. Brockhinke, K. Kohse-Höinghaus, Sampling probe influences on temperature and species concentrations in molecular beam mass spectroscopic investigations of flat premixed low-pressure flames, Z. Phys. Chem. 223 (2009) 503–537.
[53] J. Zádor, C.A. Taatjes, R.X. Fernandes, Kinetics of elementary reactions in low-temperature autoignition chemistry, Prog. Energ. Combust. 37 (2011) 371–421.
[54] X.T. Le, T.V. Mai, A. Ratkiewicz, L.K. Huynh, Mechanism and kinetics of low-temperature oxidation of a biodiesel surrogate: methyl propanoate radicals with oxygen molecule, J. Phys. Chem. A 119 (2015) 3689–3703.
[55] S.M. Sarathy, C.K. Westbrook, M. Mehl, W.J. Pitz, C. Togbe, P. Dagaut, H. Wang, M.A. Oehlschlaeger, U. Niemann, K. Seshadri, P.S. Veloo, Comprehensive chemical kinetic modeling of the oxidation of 2-methylalkanes from c7 to c20, Combust. Flame 158 (2011) 2338–2357.
[56] K. Kumar, C.J. Sung, B.W. Weber, J.A. Bunnell, Autoignition of methyl propanoate and its comparisons with methyl ethanoate and methyl butanoate, Combust. Flame 188 (2018) 116–128.
[57] Y. Zhai, B. Feng, W. Yuan, C. Ao, L. Zhang, Experimental and modeling studies of small typical methyl esters pyrolysis: Methyl butanoate and methyl crotonate, Combust. Flame 191 (2018) 160–174.
[58] A. Farooq, W. Ren, K.Y. Lam, D.F. Davidson, R.K. Hanson, Shock tube studies of methyl butanoate pyrolysis with relevance to biodiesel, Combust. Flame 159 (2012) 3235–3241.
[59] T. Tan, X. Yang, Y. Ju, E.A. Carter, Ab initio pressure-dependent reaction kinetics of methyl propanoate radicals, Phys. Chem. Chem. Phys. 17 (2015) 31061–31072.
[60] J.R. Taylor, An introduction to error analysis: Mill valley, University Science Books, 1982.
[61] B.W. Weber, C.J. Sung, M.W. Renfro, On the uncertainty of temperature estimation in a rapid compression machine, Combust. Flame 162 (2015) 2518–2528.
[62] K. Narayanaswamy, P. Pepiot, H. Pitsch, A chemical mechanism for low to high temperature oxidation of methylcyclohexane as a component of transportation fuel surrogates, Combust. Flame 162 (2015) 1193–1213.
[63] J. Yu, Y. Ju, X. Gou, Surrogate fuel formulation for oxygenated and hydrocarbon fuels by using the molecular structures and functional groups, Fuel 166 (2016) 211–218.
[64] Y. Chang, M. Jia, Y. Li, Y. Zhang, M. Xie, H. Wang, R.D. Reitz, Development of a skeletal oxidation mechanism for biodiesel surrogate, Proc. Combust. Inst. 35 (2015) 3037–3044.